well investigated. Brain endothelial cells have a receptor-mediated uptake system of α-tocopherol from α-tocopherol–containing HDL and LDL through each receptor (Goti *et al.*, 2002; Mardones *et al.*, 2002; Qian *et al.*, 2005). After α-tocopherol enters the brain, αTTP may have an important role in supplying α-tocopherol to neurons and glial cells. We and others showed that α-tocopherol in the brain was almost depleted in $\alpha TTP^{-/-}$ mice and was markedly decreased even in $\alpha TTP^{-/-}$ mice fed an α-tocopherol–rich diet resulting in increased serum α-tocopherol (Yokota *et al.*, 2001; Gohil *et al.*, 2008). αTTP is expressed in astrocytes (Hosomi *et al.*, 1998), and cholesterol, as a major lipid, is transferred to neurons and glial cells from astrocytes by HDL-like particles synthesized in astrocytes (Pfrieger, 2003; Vance *et al.*, 2005; Herz and Chen, 2006). We postulated that α-tocopherol could be delivered to neurons and glial cells by HDL-like particles in the brain. Although serum HDL and brain HDL-like particles are different in their composition and origin, their size and density are similar and both supply lipids through lipoprotein receptors with ApoE as a ligand (Vance *et al.*, 2005). Therefore, we attempted to use serum HDL as a carrier vector for α-tocopherol–conjugated siRNA to neurons and glial cells with delivery by direct ICV infusion.

Materials and Methods

siRNAs

α-Tocopherol–conjugated and Cy3-labeled siRNAs were synthesized by Hokkaido System Science (Sapporo, Japan). The sequences for the sense and antisense strands of siBACE are as follows: siBACE sense, 5′-GAAcCuAuGCGAuGCGA AuGUUUAU*A*C-3′; antisense, 5′-guauaaACAUuCGCAuC GCAUAgGUuC*U*U-3′. 2′-*O*-methyl–modified nucleotides are in lower case, and phosphorothioate linkages are represented by asterisks. α-Tocopherol and Cy3 fluorophore were covalently bound to the 5′-end of antisense and sense strands, respectively. siRNA duplexes were generated by annealing equimolar amounts of complementary sense and antisense strands.

In vitro *siRNA transfection assay*

Neuro2a cells were transfected with each siRNA at 10 n*M* with Lipofectamine RNAiMAX, as described by the vendor (Invitrogen, Carlsbad, CA). For quantitative real-time polymerase chain reaction (qRT-PCR), total RNA was extracted and 2 μg of RNA was reverse-transcribed with Superscript III kit (Invitrogen). qRT-PCR was performed using the LightCycler 480 Probes Master and LightCycler 480 II (Roche Diagnostics, Mannheim, Germany) according to the manufacturer's instructions. Primers for mouse BACE1 and glyceraldehyde-3-phosphate dehydrogenase (GAPDH) mRNAs were designed by Applied Biosystems (Foster City, CA).

For Western blot analysis, transfected cells were harvested 48 hr post transfection. Cell pellets were purified for cytosolic fraction with NE-PER nuclear and cytoplasmic extraction reagents (Thermo Fisher Scientific, Waltham, MA). Samples were separated by 10% denaturing polyacrylamide gel electrophoresis (PAGE) and transferred onto polyvinylidene difluoride membranes. Blots were probed with a rabbit antibody against BACE1 (1:500, AB5832; Millipore, Billerica, MA) and confirmed with a mouse antibody against β-tubulin (1:2000, MAB1637; Chemicon, Temecula, CA). Blots were incubated with anti-rabbit or anti-mouse secondary antibodies (1:1000) tagged with horseradish peroxidase. Blots were visualized with SuperSignal West Femto Maximum Sensitivity Substrate (Thermo Fisher Scientific) and analyzed by a ChemiDoc system (Bio-Rad, Hercules, CA).

HDL collection

The HDL fraction was prepared with sequential ultracentrifugation by a method described previously (Hatch and Lees, 1968). In brief, one volume of mouse serum and a half volume of density 1.182 solution was mixed and centrifuged for 3.5 hr at 450,000 × *g* at 16°C. A half volume of density 1.478 solution was then added to one volume of the bottom layer. The tubes were mixed and centrifuged for 4 hr, 50 min at 450,000 × *g* at 16°C. The top fraction containing HDL was used in the experiments.

HDL labeling with dipyrromethene boron difluoride

To prepare dipyrromethene boron difluoride (BODIPY) working solution, cholesteryl BODIPY 542/563 C11 powder (Invitrogen) was dissolved in dimethyl sulfoxide at a concentration of 0.5 μg/ml. The BODIPY working solution and HDL fraction were mixed at a volume ratio of 1:5 and vortexed before use.

In vitro *LDL receptor overexpression study*

HEK293T cells were grown in four-chamber slides (1×10^5 cells/well) and transfected using Lipofectamine 2000 (Invitrogen) according to the manufacturer's protocol. Briefly, 600 ng of mouse LDL receptor (LDLR; cDNA clone MGC:62289) expressing plasmid (Origene, Rockville, MD) and 60 ng pEGFP (Clontech, Mountain View, CA) or reporter plasmid alone were mixed with 1 μl of Lipofectamine 2000 and added to each well. Following 24 hr of incubation, wells were gently washed three times with Dulbecco's modified Eagle medium (DMEM), then BODIPY-labeled HDL containing DMEM (1:30 volume ratio) was added to each well and the cells were further incubated for 3 hr. After incubation, cells were fixed with 4% paraformaldehyde and nuclei were counterstained with 4′,6-diamidino-2-phenylindole.

For Western blot analysis, cells were harvested 24 hr post transfection. Cells were lysed in homogenate buffer (20 m*M* Tris-HCl [pH 7.4], 0.1% SDS, 0.1% Triton X-100, 0.01% sodium deoxycholate, 1×Complete protease inhibitor cocktail [Roche Diagnostics]). Five micrograms of total protein was separated by 10% PAGE, and the proteins were transferred onto membranes and immunoblotted as described. Blots were probed with a rabbit antibody against LDLR (1:1000; Novus Biologicals, Littleton, CO) and confirmed with a mouse antibody against GAPDH (1:3000; Chemicon).

Fluorescence correlation spectroscopy analysis

To control the total fluorescent signal under saturation, the final concentration of Toc-siRNA-Cy3 or siRNA-Cy3 was fixed at 50 n*M* and varying concentrations of unlabeled Toc-siRNA or unlabeled siRNA respectively (0 to 75 μ*M*) were added to 10-μl aliquots of the HDL fraction. Measurements were performed using the ConfoCor 3 module in combination with a LSM 510 laser scanning microscope (Carl Zeiss

MicroImaging GmbH, Göttingen, Germany) equipped with the C-Apochromat 40×/1.2W objective. A HeNe laser (543 nm) was used for Cy3-labeled siRNA excitation and emission was filtered through a 560- to 615-nm band pass filter. Samples were placed into an eight-well Lab-Tek chambered coverglass (Nalge Nunc International, Rochester, NY) and measured at room temperature. Autocorrelation curves obtained from 10 measurements with a sampling time of 20 sec were fitted with the ConfoCor 3 software package to determine diffusion time of samples.

Animals and human cerebrospinal fluid

Female Crlj:CD1 (ICR) mice aged 3 to 4 months old (27 to 30 g; Oriental Yeast, Tokyo, Japan) were used for ICV infusion experiments. For $LDLR^{-/-}$ mice, B6.129S7-Ldlr (tm1Her)/J (Jackson Laboratory, Bar Harbor, ME) and wild-type (WT) C57BL/6J (Oriental Yeast) were used. Cerebrospinal fluid was collected from a healthy human volunteer. All procedures used in animal studies and the use of human samples were approved by the ethical committee of Tokyo Medical and Dental University and were consistent with local and state regulations as applicable.

ICV infusion

Mice were anesthetized with isoflurane (1.5% to 2.0%). Osmotic minipumps (model 1007D; Alzet, Cupertino, CA) were filled with phosphate-buffered saline (PBS) or free Toc-siBACE or Toc-siBACE/HDL and connected with Brain Infusion Kit 3 (Alzet). A brain-infusion cannula was placed −0.5 mm posterior to the bregma at midline for infusion into the dorsal third ventricle (Thakker *et al.*, 2004).

Confocal immunofluorescense and histochemical microscopy analyses

The fixed brains were sectioned at 10 μm with a cryostat (Leica, Wetzlar, Germany). For confocal immunofluorescense observation, sections were immunolabeled with antibodies against MAP2 (1:200, AB5622; Chemicon) and glial fibrillary acidic protein (GFAP, 1:500, G3893; Sigma, St. Louis, MO) followed by incubation with fluorescein isothiocyanate (FITC)-conjugated secondary antibodies. Images were obtained with LSM 510 META (Zeiss). Obtained images were transmitted to image analysis software (WinROOF, Mitani, Tokyo, Japan) and analyzed to estimate the areas of each color. To examine regional BACE1 protein expression, sections were immunolabeled with a mouse monoclonal antibody (1:50, MAB5308; Chemicon) in combination with M.O.M. immunodetection kit (Vector Laboratories, Burlingame, CA) and developed with 3,3′-diaminobenzidine (DAB).

In vivo *analyses for siRNA activity*

Fresh frozen brain samples were sectioned at 10 μm and transferred onto a membrane slide (Leica), fixed, and dehydrated through a serial gradient of ethanol, 95%, 75%, 50%, 50%, 75%, 95%, 100%, for 30 sec each and once in 100% ethanol for 2 min followed by xylene for 5 min. Sample slides were set on fluorescence equipped laser microdissection system (AS LMD, Leica), and regions of interest were cut at a fixed square measure from three sections (hippocampal formation, 8.4×10^6 μm^2; parietal cortex, 5.1×10^6 μm^2). For qRT-PCR assays, total cellular RNA was extracted (PicoPure RNA isolation kit; Arcturus, Sunnyvale, CA) and total RNA was reverse-transcribed. qRT-PCR was performed as described for the *in vitro* siRNA transfection assay. For Western blots, cut samples were directly collected in 25 μl of homogenate buffer. Total proteins were separated by 10% PAGE, transferred onto membranes, and immunoblotted as described. For Northern blots, block brain samples, approximately 50 mg each, were homogenized and purified for small RNAs by MirVana (Ambion, Austin, TX). Small RNA samples were loaded 20 μg for each, separated by 24% denaturing PAGE,

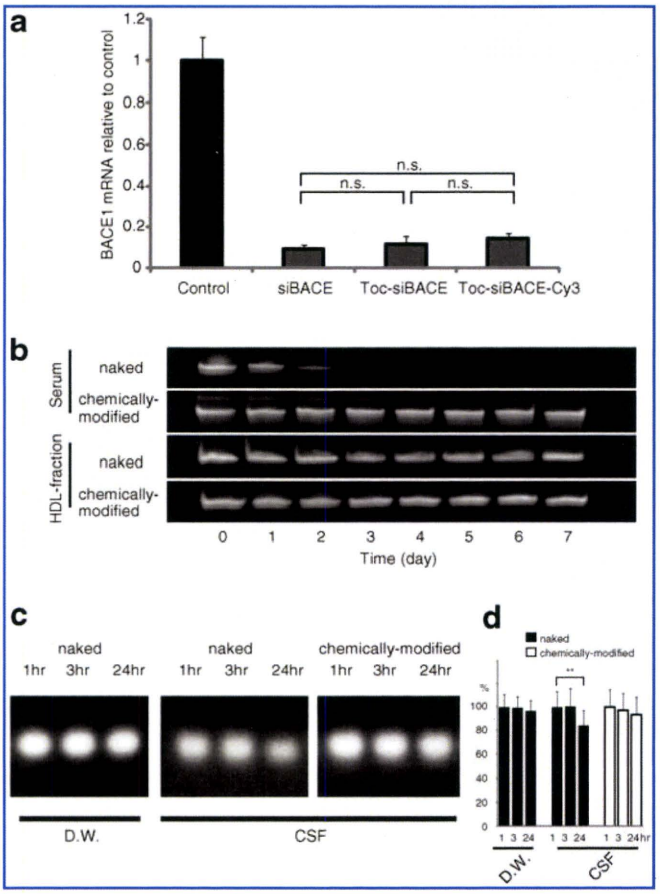

FIG. 1. *In vitro* validation of RNAi activity and stability for modified siRNAs against BACE1. **(a)** RNAi activity in mouse Neuro2a cells was measured by transfecting nonconjugated siBACE, Toc-siBACE, and Toc-siBACE-Cy3. Quantitative reverse-transcription polymerase chain reaction (qRT-PCR) analysis of BACE1 mRNA levels showed efficient target silencing after tocopherol conjugation and Cy3 labeling. (Data are shown as mean values ± SEM, $n = 3$. One-way ANOVA followed by Tukey-Kramer multiple comparisons, n.s.; not significant). **(b)** Naked siRNA or chemically modified siRNA was incubated with mouse serum or high-density lipoprotein (HDL) fraction at 37°C for up to 7 days. Samples were separated by nondenaturing 18% PAGE. **(c)** Chemically modified siRNA and naked siRNA were incubated in distilled water (D.W.) or cerebrospinal fluid (CSF) at 37°C up to 24 hr. Samples were separated on nondenaturing 2% agarose. **(d)** Densitometric analysis of the band intensities showed substantial degradation of naked siRNA in CSF. Error bars (SD) are derived from triplicates. $^{**}p < 0.01$, Student's t test.

transferred to nylon membrane (Hybond-N+, Amersham, Piscataway, NJ), and then hybridized with DNA probes labeled by DIG oligonucleotide 3′ end labeling kit (GE Healthcare, Piscataway, NJ). Signals were developed with CDP-Star (GE Healthcare).

Results

In vitro *validation of efficiency and stability of Toc-siRNA*

Using Neuro2a cells, we checked RNA interference (RNAi) activity of eight different siRNAs targeting BACE1 mRNA (NM_011792) (siBACE), two from preceding reports (Kao *et al.*, 2004; Singer *et al.*, 2005) and six newly designed sequences, and selected the best siBACE (siBACE-8) (Supplementary Fig. S1a; Supplementary data are available online at www.liebertonline.com/hum). This siBACE was confirmed to suppress endogenous BACE1 protein as well (Supplementary Fig. S1b, c).

α-Tocopherol was covalently bound to the 5′ end of the antisense strand of the siRNA. According to previously reported principles (Nishina *et al.*, 2008), we made chemical modifications with phosphorothioate backbone linkage and sugar 2′-*O*-methylation on both sense and antisense strands for increasing stability of siRNA against endogenous ribonucleases. Furthermore, 5′ end of sense strand was labeled with Cy3 fluorophore to examine histological distribution of Toc-siRNA *in vivo*.

To confirm the influence of α-tocopherol conjugation and Cy3 labeling on RNAi activity, nonconjugated siBACE, Toc-siBACE, and Cy3-labeled Toc-siBACE (Toc-siBACE-Cy3) were transfected to Neuro2a cells at 10 n*M*. These modifications did not influence silencing activity of siBACE (Fig. 1a).

To check the stability of Toc-siBACE against ribonucleases, Toc-siBACE was incubated at 37°C with mouse serum, the HDL fraction of mouse serum, or human CSF. Naked siRNA was completely degraded in serum after incubation for 3 days. Chemically modified siRNA did not degrade for up to 7 days in serum, showing satisfactory protection against ribonucleases. Naked siRNA as well as chemically modified siRNA did not degrade in the HDL fraction after 7 days, suggesting that serum ribonucleases were eliminated after sequential ultracentrifugation (Fig. 1b). With a view to direct central administration, we also checked siRNA stability in CSF. Chemically modified siRNA did not degrade in CSF (Fig. 1c). Naked siRNA showed substantial degradation in CSF after 24 hr by densitometric analysis (Fig. 1d).

Toc-siRNA binding assay with HDL

For simplicity, Toc-siRNA-Cy3 is referred to hereafter as Toc-siRNA. To demonstrate the binding of Toc-siRNA and HDL, we conducted a gel-shift assay for evaluating interaction between these two molecules.

Nonconjugated siRNA incubated with the HDL fraction migrated almost identically to that incubated with PBS. Toc-siRNA incubated with the HDL fraction showed much lower mobility than that with PBS, indicating that the interaction of Toc-siRNA with HDL was due to lipophilic binding by the tocopherol moiety of Toc-siRNA (Fig. 2a). The ratio of

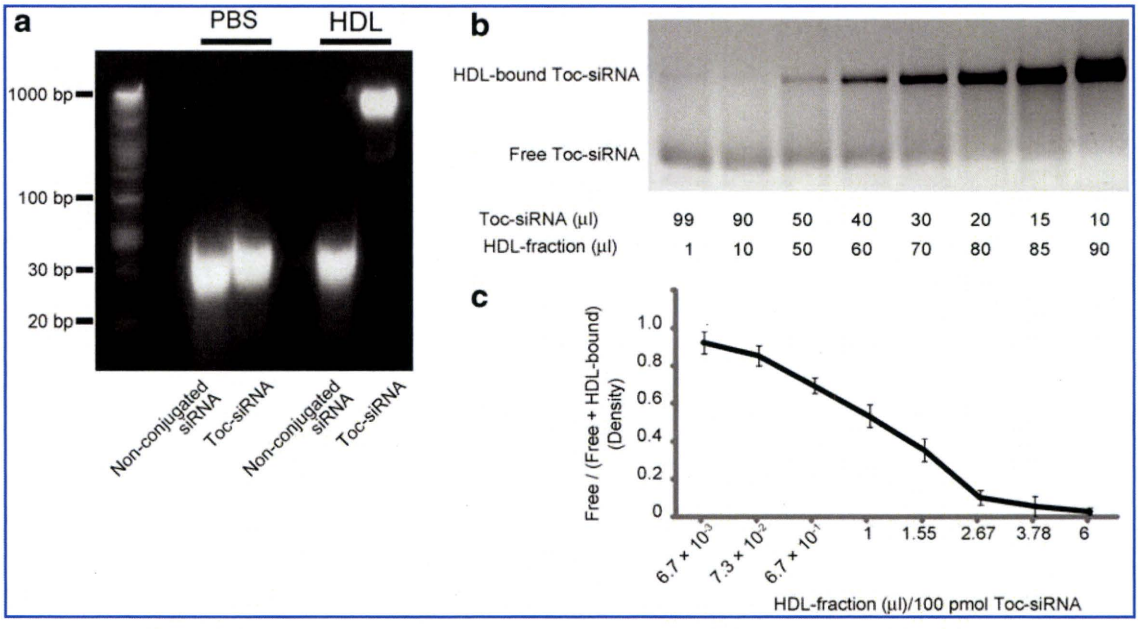

FIG. 2. Binding assay for Toc-siRNA and HDL. **(a)** 100 pmol nonconjugated siRNA or Toc-siRNA was added to 10 μl of phosphate-buffered saline (PBS) or the HDL fraction, and then samples were incubated at 37°C for 30 min. When incubated with PBS, Toc-siRNA showed slightly smaller mobility than nonconjugated siRNA on nondenaturing 2% agarose. It was assumed that the size and net charge of the molecule affected the migration change. When incubated with the HDL fraction, Toc-siRNA showed much smaller mobility than that with PBS, indicating the binding between Toc-siRNA and HDL. **(b)** Extensive gel-shift assay for Toc-siRNA and HDL binding. Varying volume ratios of 150 μM Toc-siRNA to HDL fraction were mixed and incubated at 37°C for 10 min. For a gel-shift assay, the loaded amount of Toc-siRNA was equivalent (100 pmol) for each lane and samples were separated on 2% agarose. **(c)** Densitometric analysis of free and HDL-bound Toc-siRNA. The *x*-axis shows the corresponding HDL-fraction volume in **b**. Error bars (SD) are derived from triplicates.

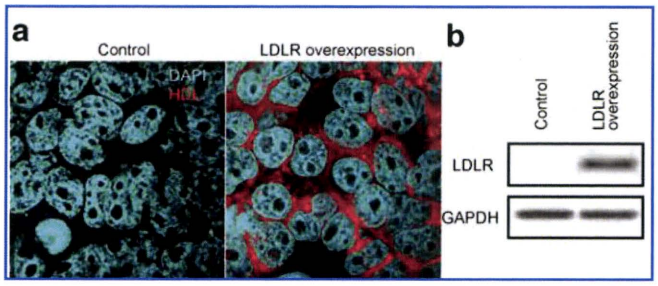

FIG. 3. Overexpression of low-density lipoprotein receptor (LDLR) facilitated HDL uptake *in vitro*. Wild-type (WT) and LDLR-overexpressed HEK293T cells were incubated with fluoro-labeled HDL (red signal). **(a)** LDLR-overexpressed cells showed intense signals of labeled HDL with dot-like cytosolic accumulation. **(b)** Western blots of HEK293T cells lysates for LDLR and GAPDH as a loading control.

Toc-siRNA to HDL fraction was determined by an extensive gel-shift assay and optical density measurements with varying ratios of Toc-siRNA to HDL fraction (Fig. 2b and c). The ratio was set at 20 μl of 150 μM Toc-siRNA to 80 μl of HDL fraction, where free Toc-siRNA almost disappeared. The binding of almost all the Toc-siRNA to HDL was also confirmed by fluorescence correlation spectroscopy analysis (Supplementary Fig. S2).

HDL uptake via LDLR in vitro

We hypothesized that serum HDL can be taken up by neurons and glial cells via LDLR because serum HDL has characteristics similar to HDL-like particles of the central nervous system (CNS) in its size, density, and apolipoproteins. To confirm this, we carried out an LDLR overexpression study *in vitro* by transfecting mouse LDLR-expressing plasmid to HEK293T cells. LDLR expression was confirmed by Western blot analysis (Fig. 3b). The mouse serum HDL fraction was labeled with fluorophore (BODIPY 542/563 C11) and applied to culture medium. LDLR-overexpressed cells showed marked HDL uptake, whereas mock-plasmid–transfected HEK293T cells as a negative control showed almost no HDL uptake (Fig. 3a).

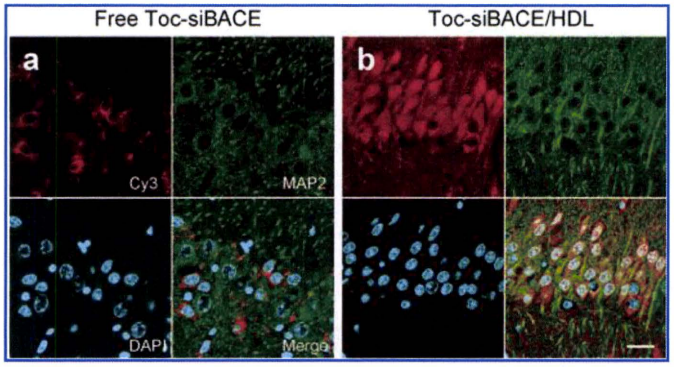

FIG. 4. Laser confocal microscopic images of MAP2-labeled hippocampus CA3 neurons infused with either **(a)** free Toc-siBACE or **(b)** Toc-siBACE/HDL. Nuclei were counterstained with 4′,6-diamidino-2-phenylindole (DAPI). Scale bar, 20 μm.

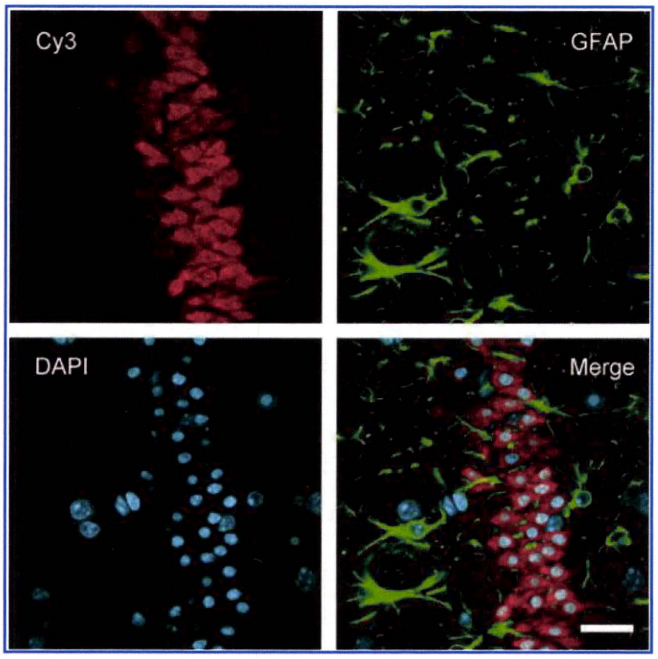

FIG. 5. Laser confocal microscopic observation for glial cell uptake of Toc-siBACE in the hippocampus CA3 region of a mouse infused with Toc-siBACE/HDL. Glial cells were detected by anti-GFAP antibody. Nuclei were counterstained with DAPI. Scale bar, 20 μm.

HDL enhanced in vivo *delivery of Toc-siRNA*

To test the performance of Toc-siRNA/HDL *in vivo*, Toc-siBACE bound to HDL was administered to the mouse brain by direct ICV infusion with osmotic pumps. Continuous ICV infusion of Toc-siBACE/HDL for 7 days achieved broader and more intense transduction of Toc-siBACE to the brain (Fig. 4b) than that of free Toc-siBACE (Fig. 4a), whereas ICV infusion of nonconjugated siBACE showed almost no signal in the brain (Supplementary Fig. S3).

The transduction of Toc-siBACE/HDL distributed broadly within the brain in the posterior frontal, parietal, and temporal areas and the hippocampal formation, and especially in areas more proximal to the lateral and third ventricles. In particular, intense signals were observed in the hippocampal neuronal cell layers and periventricular white matter.

By immunofluorescence microscopic observation, siRNA-transduced cells were mainly neuronal cells detected by anti-MAP2 antibody and showed an intense and homogenous Cy3 signal, rather than tiny dots, in the cytosol and often in the nucleus as well with Toc-siBACE/HDL–infused brain (Fig. 4b). Weaker cytosolic signal was also seen with free Toc-siBACE–infused brain (Fig. 4a). GFAP staining also depicted neuronal rather than glial uptake of Toc-siBACE in the cerebral cortex and hippocampus with Toc-siBACE/HDL–infused brain (Fig. 5).

In vivo *analyses of RNAi activity in the brain*

To measure the target mRNA reduction in the area where Toc-siRNA was transduced, we used laser dissection microscopy equipped with fluorescent observation system to capture Cy3 signal–positive regions directly. Free Toc-siBACE

could not elicit evident target gene silencing, whereas laser-dissected samples from Toc-siBACE/HDL–infused brain revealed significant reduction of target BACE1 mRNA at the hippocampal formation and parietal cortex (Fig. 6a; free Toc-siBACE vs. Toc-siBACE/HDL, hippocampus; 6% vs. 36%, parietal cortex; 13% vs. 64%, relative to control). Furthermore, neither free nontargeting Toc-siRNA (Toc-siApoB) nor Toc-siApoB/HDL affected target BACE1 mRNA level, indicating sequence specific cleavage.

Moreover, we could detect more prominent band of Dicer-cleaved antisense strand than that of the original antisense strand from Toc-siBACE/HDL–infused brain on siRNA Northern blot (Fig. 6b), indicating efficient delivery of Toc-siBACE to cytosol and its Dicer recognition.

Western blot analysis of BACE1 from signal positive regions in the parietal cortex of Toc-siBACE/HDL–infused brain showed substantial reduction of BACE1 protein (Fig. 6c and d; β-tubulin as a loading control, 52% reduction to control).

Regional repression of BACE1 protein was also evident by immunohistological examination. We could detect reduced DAB staining in the cerebral cortex, and the hippocampus, where siRNA transduction was confirmed under fluorescence microscopy (Fig. 7). Histological examination by hematoxylin-eosin (HE) staining of the Toc-siBACE/HDL–infused brain showed no obvious abnormality including cellular infiltration (Supplementary Fig. S4).

The uptake of Toc-siRNA/HDL was mediated by LDLR

Glial cells excrete ApoE-containing lipoprotein (HDL-like particles), and neurons incorporate the lipoprotein via receptor-mediated endocytosis. Several members of LDL receptor family (LDLR, low-density lipoprotein receptor-related protein 1 [LRP1], VLDL receptor [VLDLR]) are expressed in neurons and glial cells (Fan *et al.*, 2001). Amongst these receptors, LDLR is a cardinal one for metabolism of HDL-like particles (Vance *et al.*, 2005). We used $LDLR^{-/-}$ mice to see whether Toc-siRNA/HDL uptake is mediated by this receptor. $LDLR^{-/-}$ mice infused with Toc-siBACE/HDL showed much less Cy3 signals in the hippocampal neuronal cell layers than WT mice (Fig. 8a). In the periventricular

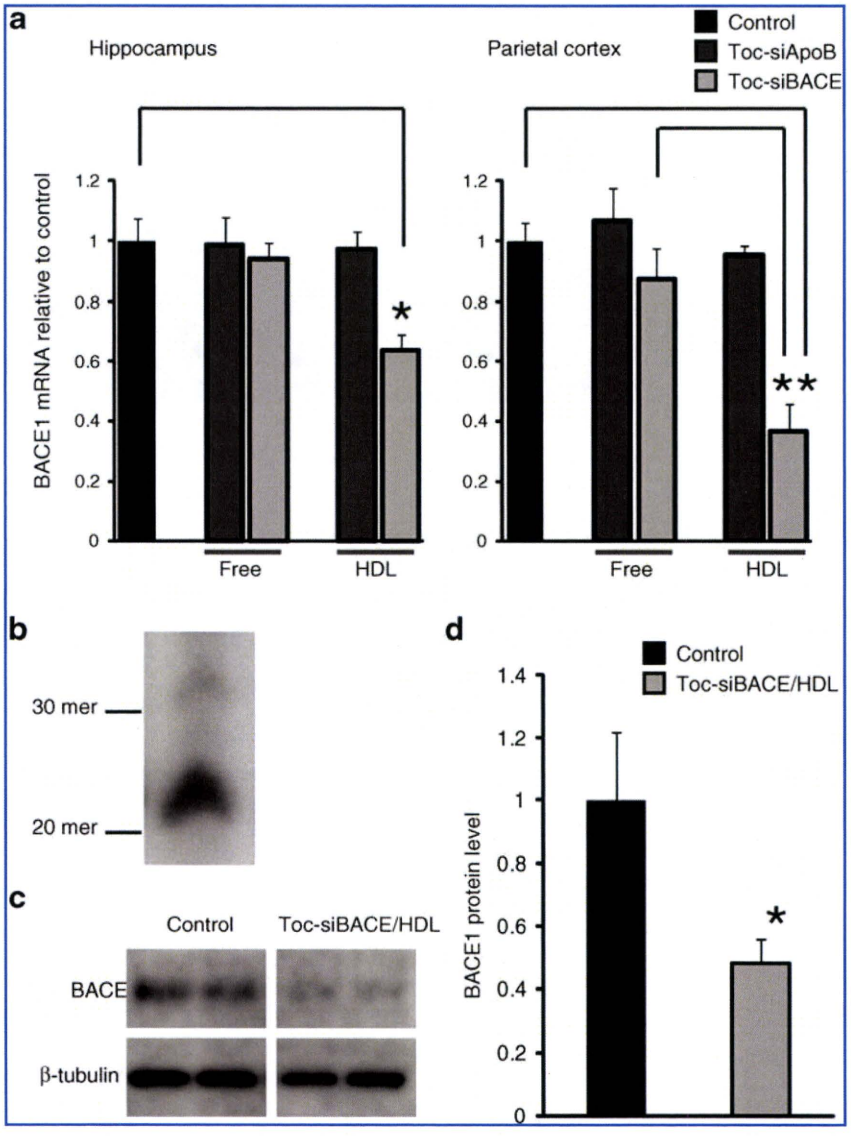

FIG. 6. *In vivo* analyses of RNAi activity of free Toc-siBACE and Toc-siBACE/HDL. **(a)** For qRT-PCR analyses, mRNA was purified from laser-dissected samples of the same square measure from each brain region of control brains (PBS infusion), free Toc-siRNA–infused or Toc-siRNA/HDL–infused brains. (Data are shown as mean values ± SEM, $n = 3$. One-way ANOVA followed by Tukey-Kramer multiple comparisons, $^{*}p < 0.05$, $^{**}p < 0.01$). **(b)** Northern blot analysis for Toc-siBACE. Small RNAs were purified from total homogenate of a 3-mm-thick brain section adjacent to the infusion site of the brain. Membrane was proved with the DIG-labeled DNA oligonucleotides of the sense strand. **(c)** For Western blot, total lysates of laser dissected samples of the same square measure from the parietal cortex region were immunoblotted with anti-BACE1 antibody and confirmed with anti-β-tubulin antibody as a loading control. **(d)** Bar graph shows BACE1/tubulin ratios from densitometry of bands in **c**. Values represent mean ± SEM. $^{*}p = 0.092$, Student's t test.

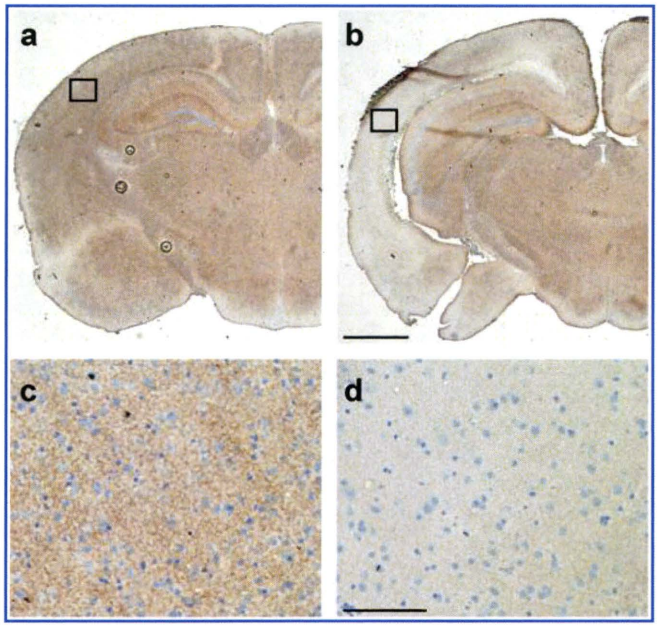

FIG. 7. Regional suppression of BACE1 protein by Toc-siBACE/HDL. **(a)** PBS-infused or **(b)** Toc-siBACE/HDL–infused brain sections were immunoperoxidase-stained for BACE1. Reduced DAB staining in the entorhinal, parietal cortex, and hippocampus is shown. Scale bar, 500 μm. **(c, d)** Panels show insets in **a** and **b**, respectively. Scale bar, 50 μm.

white matter regions, despite the similar level of Cy3 signals from the extracellular space (red) between WT and LDLR$^{-/-}$ mice, Cy3-positive areas in astrocytes as shown in merged yellow were decreased for LDLR$^{-/-}$ mice compared with WT mice (Fig. 8b). When normalized to the total GFAP-positive green area, the decrease in glial uptake of Toc-siBACE/HDL in LDLR$^{-/-}$ mice was statistically significant (Fig. 8c; WT vs. LDLR$^{-/-}$, 0.306 ± 0.082 vs. 0.096 ± 0.05, $p = 0.019$).

Discussion

The ability to direct a particular class of drugs to the brain has been desired for years, but the existence of the blood–brain barrier and the peculiar metabolism of the brain are major obstacles for drug delivery. In this study we developed a new and efficient method of delivering siRNA to the brain by conjugating it with α-tocopherol and HDL. Our vector system significantly lowered the dose of siRNA needed for silencing the target mRNA in the CNS.

Similar gene-silencing trials with ICV infusion of non-conjugated siRNA with chemical modifications have been reported (Senn *et al.*, 2005; Senechal *et al.*, 2007). The ICV infusion of free siRNA against dopamine receptor DDAR into the third ventricle of the mouse brain for 7 days could suppress the target mRNA by 60% with phenotypic change (Thakker *et al.*, 2004). Thakker *et al.*, (2004) reported the dose of free siRNA needed was as much as 3 μmol, whereas we found that just 3 nmol of Toc-siRNA with HDL could induce a target reduction in comparable degree by the same ICV infusion method. The *in vivo* knockdown using antisense oligonucleotides by its ICV infusion was also studied over the last two decades (Godfray and Estibeiro, 2003). Generally, ICV infused antisense oligonucleotides were more readily taken up by brain tissues than free siRNA, but their silencing efficacy is lower than free siRNA (Senn *et al.*, 2005). For example, 4.7 μmol of an ICV infusion of antisense oligonucleotides to superoxide dismutase 1 was needed to achieve 60% reduction of the target mRNA in the brain (Smith *et al.*, 2006). Roughly speaking, we could get a similar level of silencing effect in the brain with about a 1000-fold lower amount of siRNA with our method compared with ICV infused free siRNA or antisense oligonucleotides. The

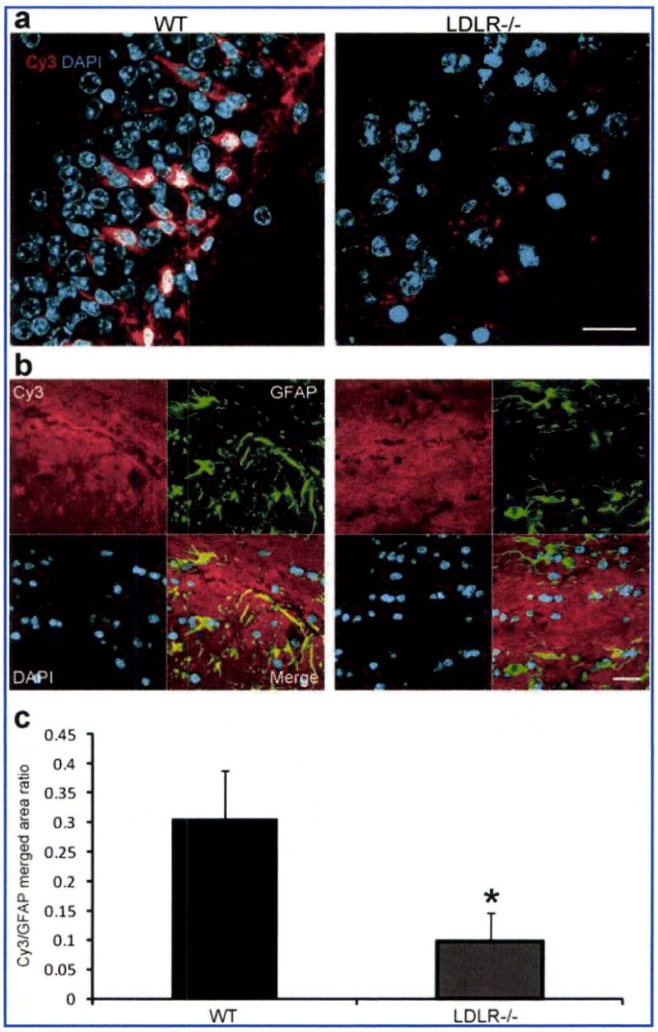

FIG. 8. Neuronal and glial uptake of Toc-siRNA/HDL mediated by LDL receptor. WT and LDLR$^{-/-}$ mice were intracerebroventricular (ICV) infused with Toc-siBACE/HDL for 7 days. **(a)** Confocal fluorescence observation revealed reduced uptake of Toc-siBACE/HDL in pyramidal neurons in the hippocampus CA3 of LDLR$^{-/-}$ mice compared with WT. Scale bar, 20 μm. **(b)** Immunofluorescence confocal observation for glial cells at corpus callosum of WT and LDLR$^{-/-}$ mice. Glial cells were detected by GFAP staining. Scale bar, 20 μm. **(c)** Bar graph shows Toc-siRNA/HDL uptake area ratio in glial cells from WT and LDLR$^{-/-}$ mice. GFAP and Cy3 positive yellow areas are divided by GFAP-positive green areas. WT, $n = 3$. LDLR$^{-/-}$, $n = 3$. Values represent mean $\pm$ SD. *$p = 0.019$, Student's t test.

direct intraparenchymal brain injection of naked siRNA (Querbes *et al.*, 2009), siRNA with cationic vector (Wang *et al.*, 2005), or cholesterol-conjugated siRNA (DiFiglia *et al.*, 2007) was also studied, but the distribution of siRNA was limited and the procedures were more invasive.

As the cause for our better RNAi effect, we think that our vector system utilizes the physiological lipid metabolism in the brain. The CNS has HDL-like particles that are synthesized mainly by astrocytes to mediate transport of lipids to neurons and glial cells (Vance *et al.*, 2005; Fünfschilling *et al.*, 2007). Since α-tocopherol is a highly lipophilic molecule and astrocytes express αTTP, we assumed that α-tocopherol is transferred from glial cells to neurons via the receptor-mediated pathway with HDL-like particles.

HDL-like particles in the brain contain ApoE as a major apolipoprotein, which is to be the ligand for the receptor-mediated endocytosis by LDLR and LRP1 in neurons (Rothe and Müller, 1991; Posse *et al.*, 2000). In addition, astrocytes also express LDLR and LRP-1 (LaDu, 2000; Rapp *et al.*, 2006) and internalize HDL-like particles. HDL-like particles and serum HDL are similar to each other in density and size, and both have ApoE and ApoA-1 (Pitas *et al.*, 1987). Since it was shown that rat sympathetic neurons can take up serum LDL and HDL as well as HDL-like particles via its LDLR (Rothe and Müller, 1991), we used serum HDL as a vector to deliver Toc-siRNA to neurons. Significant knockdown of endogenous BACE1 mRNA by ICV infusion of Toc-siRNA/HDL could not be obtained without binding to HDL, and moreover the delivery was much lower in $LDLR^{-/-}$ mouse brains. With these results, we believe that this vector system utilizes the physiological receptor-mediated lipid metabolism pathway of the brain, but not simple diffusion or macropinocytosis, to deliver siRNA. However, the uptake of Toc-siRNA/HDL in $LDLR^{-/-}$ mice was not completely diminished, suggesting that other lipoprotein receptors such as LRP1 or megalin, or another uptake mechanism of siRNA, such as a SID-1–mediated pathway in hepatocytes (Duxbury *et al.*, 2005), might contribute to the remaining uptake.

Although the delivery efficiency of siRNA by our vector system is better than previously reported, the reduction of the target mRNA of BACE1 was as much as 60% to 70%. Even partial reduction of BACE1, however, is suggested to have a dramatic effect on Alzheimer pathology in AD model mice with mutant amyloid precursor protein (APP). Single allele ablation caused only a 12% decrease in Aβ level, but nonetheless resulted in four- to fivefold fewer Aβ plaques (McConlogue *et al.*, 2007). Similarly, only 40% reduction of BACE1 protein by directly injected siRNA-expressing lentivirus significantly reduced AD pathology (Singer *et al.*, 2005). Additionally, duplication of the *APP* gene with a 1.5-fold gene dosage increase is known to cause familial AD (Blom *et al.*, 2008), suggesting that a 33% reduction of APP expression is enough to prevent the disease. Therefore, a more than 60% reduction of BACE1 with our vector system can be expected to reduce Aβ load and improve AD phenotype.

Together, we could achieve highly efficient gene silencing in the brain by ICV infusion of Toc-siRNA/HDL that should utilize the receptor-mediated physiological pathway. That resulted in lower doses by orders of magnitude than needed in previously reported methods for nucleotide delivery to the brain.

Acknowledgments

This work was supported by grants from the Japanese Society for the Promotion of Science (#20023010) and the Japan Foundation for Neuroscience and Mental Health (#2212070).

Author Disclosure Statement

The authors declare no competing financial interests.

References

Akinc, A., Goldberg, M., Qin, J., *et al.* (2009). Development of lipidoid-siRNA formulations for systemic delivery to the liver. Mol. Ther. 17, 872–879.

Akinc, A., Zumbuehl, A., Goldberg, M., *et al.* (2008). A combinatorial library of lipid-like materials for delivery of RNAi therapeutics. Nat. Biotechnol. 5, 561–569.

Blom, E.S., Viswanathan, J., Kilander, L., *et al.* (2008). Low prevalence of APP duplications in Swedish and Finnish patients with early-onset Alzheimer's disease. Eur. J. Hum. Genet. 2, 171–175.

DiFiglia, M., Sena-Esteves, M., Chase, K., *et al.* (2007). Therapeutic silencing of mutant huntingtin with siRNA attenuates striatal and cortical neuropathology and behavioral deficits. Proc. Natl. Acad. Sci. U. S. A. 43, 17204–17209.

Duxbury, M.S., Ashley, S.W., and Whang, E.E. (2005). RNA interference: a mammalian SID-1 homologue enhances siRNA uptake and gene silencing efficacy in human cells. Biochem. Biophys. Res. Commun. 2, 459–463.

Fan, Q., Iosbe, I., Asou, H., *et al.* (2001). Expression and regulation of apolipoprotein E receptors in the cells of the central nervous system in culture: A review. J. Am. Aging. Assoc. 24, 1–10.

Fünfschilling, U., Saher, G., Xiao, L., *et al.* (2007). Survival of adult neurons lacking cholesterol synthesis in vivo. BMC Neurosci. 8, 1.

Gao, S., Dagnaes-Hansen, F., Nielsen, E.J., *et al.* (2009). The effect of chemical modification and nanoparticle formulation on stability and biodistribution of siRNA in mice. Mol. Ther. 7, 1225–1233.

Godfray, J., and Estibeiro, P. (2003). The potential of antisense as a CNS therapeutic. Expert Opin. Ther. Targets. 3, 363–376.

Gohil, K., Oommen, S., Quach, H.T., *et al.* (2008). Mice lacking alpha-tocopherol transfer protein gene have severe alpha-tocopherol deficiency in multiple regions of the central nervous system. Brain Res. 1201, 167–176.

Goti, D., Balazs, Z., Panzenboeck, U., *et al.* (2002). Effects of lipoprotein lipase on uptake and transcytosis of low density lipoprotein (LDL) and LDL-associated alpha-tocopherol in a porcine in vitro blood-brain barrier model. J. Biol. Chem. 32, 28537–28544.

Hatch, F.T., and Lees, R.S. (1968). Practical methods for plasma lipoprotein analysis. Advan. Lipid Res. 6, 1–68.

Herz, J., and Chen, Y. (2006). Reelin, lipoprotein receptors and synaptic plasticity. Nat. Rev. Neurosci. 11, 850–859.

Hosomi, A., Goto, K., Kondo, H., *et al.* (1998). Localization of alpha-tocopherol transfer protein in rat brain. Neurosci. Lett. 3, 159–162.

Kao, S.C., Krichevsky, A.M., Kosik, K.S., and Tsai, L.H. (2004). BACE1 suppression by RNA interference in primary cortical neurons. J. Biol. Chem. 3, 1942–1949.

Kappus, H., and Diplock, A.T. (1992). Tolerance and safety of vitamin E: a toxicological position report. Free Radic. Biol. Med. 1, 55–74.

Kim, D.H., Behlke, M.A., Rose, S.D., *et al.* (2005). Synthetic dsRNA Dicer substrates enhance RNAi potency and efficacy. Nat. Biotechnol. 2, 222–226.

Kumar, P., Wu, H., McBride, J.L., *et al.* (2007). Transvascular delivery of small interfering RNA to the central nervous system. Nature 7149, 39–43.

LaDu, M.J. (2000). Apolipoprotein E receptors mediate the effects of beta-amyloid on astrocyte cultures. J. Biol. Chem. 43, 33974–33980.

Lima, W.F., Murray, H., Nichols, J.G., *et al.* (2009). Human Dicer binds short single-strand and double-strand RNA with high affinity and interacts with different regions of the nucleic acids. J. Biol. Chem. 4, 2535–2548.

Mardones, P., Strobel, P., Miranda, S., *et al.* (2002). Alpha-tocopherol metabolism is abnormal in scavenger receptor class B type I (SR-BI)-deficient mice. J. Nutr. 3, 443–449.

McConlogue, L., Buttini, M., Anderson, J.P., *et al.* (2007). Partial reduction of BACE1 has dramatic effects on Alzheimer plaque and synaptic pathology in APP Transgenic Mice. J. Biol. Chem. 282, 26326–26334.

Moschos, S.A., Williams, A.E., and Lindsay, M.A. (2007). Cell-penetrating-peptide-mediated siRNA lung delivery. Biochem. Soc. Trans. 4, 807–810.

Nishina, K., Unno, T., Uno, Y., *et al.* (2008). Efficient in vivo delivery of siRNA to the liver by conjugation of alpha-tocopherol. Mol. Ther. 4, 734–740.

Pfrieger, F.W. (2003). Cholesterol homeostasis and function in neurons of the central nervous system. Cell Mol. Life Sci. 6, 1158–1171.

Pitas, R.E., Boyles, J.K., Lee, S.H., *et al.* (1987). Lipoproteins and their receptors in the central nervous system. J. Biol. Chem. 29, 14352–14360.

Posse De Chaves, E.I., Vance, D.E., Campenot, R.B., *et al.* (2000). Uptake of lipoproteins for axonal growth of sympathetic neurons. J. Biol. Chem. 26, 19883–19890.

Qian, J., Morley, S., Wilson, K., *et al.* (2005). Intracellular trafficking of vitamin E in hepatocytes: the role of tocopherol transfer protein. J. Lipid Res. 10, 2072–2082.

Querbes, W., Ge, P., Zhang, W., *et al.* (2009). Direct CNS Delivery of siRNA Mediates Robust Silencing in Oligodendrocytes. Oligonucleotides 1, 23–30.

Rapp, A., Gmeiner, B., and Hüttinger, M. (2006). Implication of apoE isoforms in cholesterol metabolism by primary rat hippocampal neurons and astrocytes. Biochimie 5, 473–483.

Rigotti, A. (2007). Absorption, transport, and tissue delivery of vitamin E. Mol. Aspects Med. 5–6, 423–436.

Rothe, T., and Müller, H.W. (1991). Uptake of endoneurial lipoprotein into Schwann cells and sensory neurons is mediated by low density lipoprotein receptors and stimulated after axonal injury. Neurochem. 6, 2016–2025.

Rozema, D.B., Lewis, D.L., Wakefield, D.H., *et al.* (2007). Dynamic PolyConjugates for targeted in vivo delivery of siRNA to hepatocytes. Proc. Natl. Acad. Sci. USA. 32, 12982–12987.

Senechal, Y., Kelly, P.H., Cryan, J.F., *et al.* (2007). Amyloid precursor protein knockdown by siRNA impairs spontaneous alternation in adult mice. J. Neurochem. 6, 1928–1940.

Senn, C., Hangartner, C., Moes, S., *et al.* (2005). Central administration of small interfering RNAs in rats: a comparison with antisense oligonucleotides. Eur. J. Pharmacol. 1–3, 30–37.

Singer, O., Marr, R.A., Rockenstein, E., *et al.* (2005). Targeting BACE1 with siRNAs ameliorates Alzheimer disease neuropathology in a transgenic model. Nat. Neurosci. 10, 1343–1349.

Smith, R.A., Miller, T.M., Yamanaka, K., *et al.* (2006). Antisense oligonucleotide therapy for neurodegenerative disease. J. Clin. Invest. 8, 2290–2296.

Thakker, D.R., Natt, F., Hüsken, D., *et al.* (2004). Neurochemical and behavioral consequences of widespread gene knockdown in the adult mouse brain by using nonviral RNA interference. Proc. Natl. Acad. Sci. USA. 49, 17270–17275.

Vance, J.E., Hayashi, H., and Karten, B. (2005). Cholesterol homeostasis in neurons and glial cells. Semin. Cell Dev. Biol. 2, 193–212.

Wang, Y.L., Liu, W., Wada, E., *et al.* (2005). Clinico-pathological rescue of a model mouse of Huntington's disease by siRNA. Neurosci. Res. 3, 241–249.

Wolfrum, C., Shi, S., Jayaprakash, K.N., *et al.* (2007). Mechanisms and optimization of in vivo delivery of lipophilic siRNAs. Nat. Biotechnol. 10, 1149–1157.

Yokota, T., Igarashi, K., Uchihara, T., *et al.* (2001). Delayed-onset ataxia in mice lacking alpha-tocopherol transfer protein: model for neuronal degeneration caused by chronic oxidative stress. Proc. Natl. Acad. Sci. USA. 26, 15185–15190.

Yu, L., Tan, M., Ho, B., *et al.* (2006). Determination of critical micelle concentrations and aggregation numbers by fluorescence correlation spectroscopy: aggregation of a lipopolysaccharide. Anal. Chim. Acta 1, 216–225.

Zimmermann, T.S., Lee, A.C., Akinc, A., *et al.* (2006). RNAi-mediated gene silencing in non-human primates. Nature 441, 111–114.

Address correspondence to:
Takanori Yokota
Department of Neurology and Neurological Science
Tokyo Medical and Dental University
1-5-45 Yushima
Bunkyo-ku
Tokyo 113-8519
Japan

E-mail: tak-yokota.nuro@tmd.ac.jp

Received for publication November 7, 2010;
accepted after revision December 17, 2010.

Published online: December 17, 2010.

LGI3 interacts with flotillin-1 to mediate APP trafficking and exosome formation

Sachi Okabayashi[a,b] and Nobuyuki Kimura[a]

We recently showed that leucine-rich glioma inactivated 3 (LGI3) mediates the internalization of β-amyloid protein and transferrin, a well-known marker for clathrin-dependent endocytosis, in neural cells. These findings strongly suggest that LGI3 is involved in the endocytosis system in the brain; however, the precise function of LGI3 remains unclear. Here, we show that LGI3 interacts with flotillin-1 (Flo1), and RNA interference analysis shows that LGI3 stabilized Flo1, and Flo1 also stabilized LGI3 *vice versa*. Moreover, the downregulation of the LGI3/Flo1 complex altered β-amyloid precursor protein trafficking directly to late endosomes and disrupted exosome formation, suggesting that LGI3 is involved not only in endocytosis but also in another intracellular transport system through binding with its co-factor such as Flo1. *NeuroReport* 21:606–610 © 2010 Wolters Kluwer Health | Lippincott Williams & Wilkins.

NeuroReport 2010, 21:606–610

Keywords: β-amyloid precursor protein, clathrin, endocytosis, flotillin-1, leucine-rich glioma inactivated 3

[a]Laboratory of Disease Control, Tsukuba Primate Research Center, National Institute of Biomedical Innovation and [b]The Corporation for Production and Research of Laboratory Primates, Hachimandai, Tsukuba-shi, Ibaraki, Japan

Correspondence to Dr Nobuyuki Kimura, PhD, DVM, Laboratory of Disease Control, Tsukuba Primate Research Center, National Institute of Biomedical Innovation, 1-1 Hachimandai, Tsukuba-shi, Ibaraki 305-0843, Japan
Tel: +81 29 837 2121; fax: +81 29 837 0218; e-mail: kimura@nibio.go.jp

Received 20 January 2010 **accepted** 31 January 2010

Introduction

We have shown earlier that β-amyloid protein (Aβ) upregulates leucine-rich glioma inactivated 3 (LGI3) in cultured rat astrocytes [1]. Aβ is the major component of senile plaques, which are a characteristic feature of Alzheimer's disease [2]. Recently, we showed that LGI3 mediates the internalization of Aβ and transferrin, a well-known marker for clathrin (CLA)-dependent endocytosis in neural cells [3].

These findings strongly suggest that LGI3 is involved in the endocytosis system in the brain.

How glial cells take up Aβ remains controversial, and a recent study showed that Aβ internalization does not depend on CLA or caveolae [4]. Flotillin-1 (Flo1) is associated with noncaveolar membrane microdomains and has been recently shown to be a defining component of a CLA-independent and caveolin-independent endocytic pathway in mammalian cells [5]. Thus, in this study, we investigated the relationship between LGI3 and Flo1 or CLA. Here, we show that LGI3 interacts with Flo1 in the brain, and RNA interference studies showed that the LGI3/Flo1 complex mediates β-amyloid precursor protein (APP) trafficking and exosome formation.

Methods

Co-immunoprecipitation

C57BL/6 mice were purchased from SLC Japan (Shizuoka, Japan), and cortices from 10-week-old mice were used for co-immunoprecipitation in this study.

All steps were performed at 4°C unless otherwise noted. For immunoprecipitation, we used Dynabeads Protein G (Invitrogen, Carlsbad, California, USA). Mouse brains were homogenized in lysis buffer consisting 25 mM Tris–HCl (pH 8.0), 0.5% Triton X-100, 0.5% Nonidet P-40, and a Complete Mini proteinase inhibitor cocktail, and then centrifuged at 100 000*g* for 15 min. The precleaned supernatant containing 500 μg of proteins was incubated with goat polyclonal anti-Flo1 (Flo1g; Santa Cruz Biotechnology, Santa Cruz, California, USA) or goat IgG (Southern Biotechnology, Birmingham, Alabama, USA) for 2 h. After immunoreaction, the antibody-linked supernatant was incubated with precleaned beads for 1 h. The protein was eluted from the beads with an electrophoresis sample buffer, and then subjected to western blot analyses as described earlier [1]. We used the following primary antibodies: rabbit polyclonal anti-LGI3 [1] and rabbit polyclonal anti-Flo1 (Flo1r; Santa Cruz Biotechnology). We performed three independent experiments by using different mouse brains (see Supplementary Figure, Supplemental digital content 1, *http://links.lww.com/WNR/A52*).

All animal experiments were carried out according to the National Institute of Biomedical Innovation rules and guidelines for experimental animal welfare.

RNA interference

Mouse neuroblastoma Neuro2a cells were cultured in a culture medium (Dulbecco's Modified Eagle's Medium with 10% fetal calf serum). The cells were plated at 1.5×10^4 cells/cm^2 onto 12-well plates (Wako, Osaka, Japan) for

Supplemental digital content is available for this article. Direct URL citations appear in the printed text and are provided in the HTML and PDF versions of this article on the journal's Website (*www.neuroreport.com*).

0959-4965 © 2010 Wolters Kluwer Health | Lippincott Williams & Wilkins

DOI: 10.1097/WNR.0b013e3283383467

western blot analyses, or plated at 1.0×10^4 cells/cm^2 onto 2-well LAB-TEK chamber slides (Nalge Nunc, Rochester, New York, USA) for immunocytochemistry.

For double-stranded RNA-mediated interference (RNAi) studies, we used the following short double-stranded RNAs (siRNAs) against LGI3 (siLGI3), Flo1 (siFlo1), and clathrin heavy chain (siCLA): siLGI3, 5′-CCGUUGC UAGCGUGUCUGAGU-3′ (sense) and 5′-UCAGACACG CUAGCAACGGAG-3′ (antisense); siFlo1, 5′-CUAGUGG AAGCGGAACCAUGG-3′ (sense) and 5′-AUGGUUCCG CUUCCACUAGAC-3′ (antisense); siCLA, 5′-GCUACU UAGUCCGUCGAAAGG-3′ (sense) and 5′-UUUCGACG GACUAAGUAGCGA-3′ (antisense). To avoid off-target effects, all siRNAs were carefully designed by Enhanced siDirect. The control siRNA had a random sequence. RNAi experiments were performed by using siLentFect lipid reagent (BioRad, Hercules, California, USA), according to the manufacturer's protocol.

Seventy-two hours after siRNA transfection, cells (12-well plates) were lysed in a sample buffer solution containing 62.5 mM Tris–HCl (pH 6.8), 2 mM EDTA, 0.5% Triton X-100, 2% SDS, and proteinase inhibitor cocktail to extract total cellular proteins. Total proteins were adjusted to 10 μg, and then subjected to western blot analyses. We used the following primary antibodies: anti-LGI3 [1]; mouse monoclonal anti-β-actin (Sigma, St Louis, Missouri, USA); anti-Flo1r; anti-CLAm; rabbit polyclonal anti-APP (Zymed, Carlsbad, California, USA); mouse monoclonal antisecreted fragment of APP by α-secretase (sAPPα; IBL, Gunma, Japan); and rabbit polyclonal anti-secreted fragment of APP by β-secretase (sAPPβ; IBL). The anti-APP antibody used in this study recognizes both full-length APP and C-terminal fragment of APP by α-secretase (αCTF) or β-secretase (βCTF). Immunoreactive bands were quantified with commercially available software (Quantity One, PDI, Inc., Upper Saddle River, New Jersey, USA), and one-way analyses of variance were performed followed by the Bonferroni/Dunn post-hoc test. We performed three independent experiments ($N = 6$ for each experimental group), duplicating each experiment.

Cells plated on chamber slides were fixed with 4% paraformaldehyde and then permeabilized with 0.5% Tween 20. After blocking with 3% bovine serum albumin, the cells were incubated overnight at 4°C with the following primary antibodies: anti-LGI3; anti-Flo1g; anti-CLAm; anti-APP; rabbit polyclonal anti-sortilin (Applied Biological Materials, Richmond, Canada); rabbit polyclonal anti-TrkB (Santa Cruz Biotechnology); mouse monoclonal anti-Rab7 (Abcam, Cambridge, Massachusetts, USA); and mouse monoclonal anti-Golgi (Abcam). The cells were then incubated with AlexaFluor-conjugated secondary antibodies (Invitrogen), followed by a DAPI nuclear stain (Santa Cruz Biotechnology) for 1 h at room temperature. All cells were examined with a Digital Eclipse C1 confocal microscope (Nikon, Kanagawa, Japan).

Preparation of extracellular membrane fractions and immunoblotting for medium-derived sAPPα

Seventy-two hours after siRNA treatment, extracellular membrane fractions were prepared from the culture medium (12-well plates) as described elsewhere [6]. The resulting pellets were resuspended in the sample buffer, and then subjected to western blot analyses. We used the following primary antibodies: mouse monoclonal anti-Alix (Santa Cruz Biotechnology), anti-Flo1r, and mouse monoclonal anti-transferrin receptor (TfR; Zymed). In addition, to assess the levels of sAPPα secreted from the cells, culture media were subjected to ultracentrifugation at 100 000*g* for 1 h. The resulting pellets were resuspended in the sample buffer, and then subjected to immunoblotting with anti-sAPPα1. We examined 12 independent samples for each group.

Results

LGI3 interacts with Flo1 in the brain

In mouse neuroblastoma Neuro2a cells, Flo1 almost completely colocalized with LGI3; however, CLA partly colocalized with LGI3 near the plasma membrane (Fig. 1a). To assess whether LGI3 interacts with Flo1 *in vivo*, we performed co-immunoprecipitation using mouse brain homogenates. In the mouse brain, several anti-LGI3-specific immunoreactive bands were detected as reported earlier [7], and an approximately 70 kDa form of LGI3 was immunoprecipitated with an anti-Flo1 antibody (Fig. 1b).

Next, we performed RNAi studies to assess whether LGI3 is required for the stability of the complex. Western blot analyses confirmed that our siRNAs successfully downregulated each target in the Neuro2a cells (Fig. 1c). The depletion of LGI3 induced significant downregulation of Flo1, and the depletion of Flo1 also induced downregulation of LGI3 and *vice versa* (Fig. 1c). By contrast, we did not observe such a relationship between LGI3 and CLA (Fig. 1c). Immunocytochemistry confirmed that the Flo1 immunoreactivity diminished in LGI3-depleted cells, whereas CLA immunoreactivity persisted (data not shown).

LGI3/Flo1 complex mediates APP trafficking

Flo1 is associated with a lipid raft, and growing evidence suggests that lipid raft-associated proteins mediate APP endocytosis and cleavage [8–10]. These findings prompted us to investigate whether the LGI3/Flo1 complex mediates APP endocytosis and/or cleavage. As APP cleavage by β-secretase mainly occurs through an endocytic pathway [7], we first investigated the sAPPβ and βCTF levels. The depletion of Flo1 or LGI3 clearly decreased the amount of both sAPPβ and βCTF (Fig. 2a and b).

Fig. 1

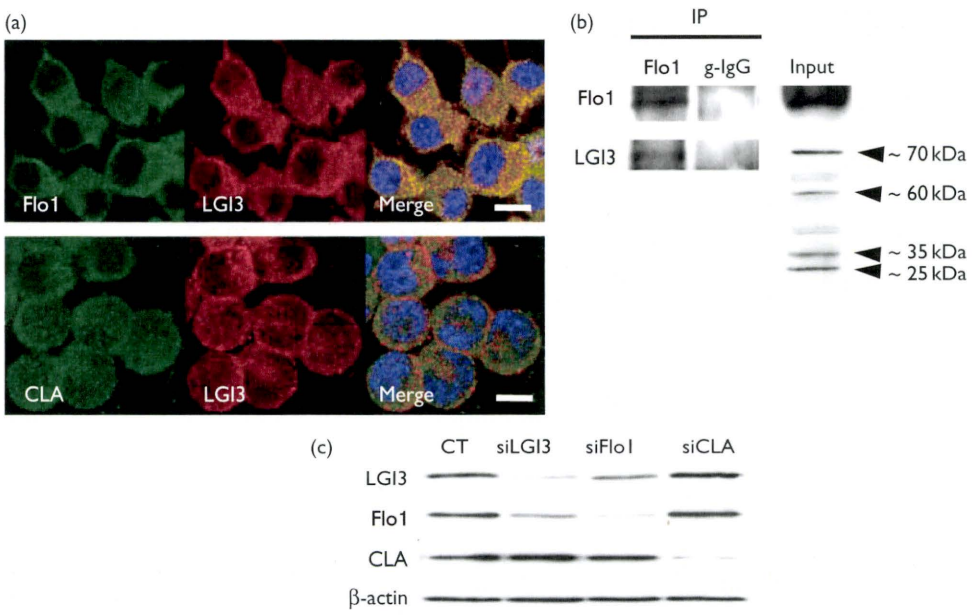

(a) Photomicrographs of Neuro2a cells immunostained for LGI3, Flo1, and CLA. Flo1 almost completely colocalized with LGI3, however, CLA partly colocalized with LGI3 near plasma membrane. Scale bars, 10 μm. (b) In mouse brain, several anti-LGI3-specific immunoreactive bands were detected, and co-immunoprecipitation analysis showed that a 70 kDa (approx.) form of LGI3 interacts with Flo1; g-IgG, control goat IgG. (c) Western blots showing the amount of LGI3, Flo1, CLA, and β-actin in extracts from Neuro2a cells 72 h after siRNA treatment. The amount of LGI3, Flo1, and CLA clearly dropped 72 h after transfection with each specific siRNA, respectively. The depletion of LGI3 resulted in the concurrent downregulation of Flo1, and the depletion of Flo1 also induced downregulation of LGI3 vice versa. CT, cells transfected with control siRNA; siLGI3, cells transfected with siLGI3; siFlo1, cells transfected with siFlo1; siCLA, cells transfected with siCLA.

APP can be alternately cleaved by α-secretase at plasma membranes [11]. Unexpectedly, the depletion of Flo1 or LGI3 also decreased the amount of both sAPPα and αCTF (Fig. 2a and b). We also confirmed the decrease of sAPPα released into the culture medium (Fig. 2c).

Immunocytochemistry showed that the depletion of LGI3 altered the intracellular localization of APP, and APP clearly accumulated near the nucleus in LGI3-depleted cells (Fig. 2d). Double immunocytochemistry showed that the accumulated APP is localized to Rab7-positive endosomes (Fig. 2d) but not to Golgi (data not shown). The depletion of LGI3 did not alter the localization of sortilin (Fig. 2d) or TrkB (data not shown).

LGI3/Flo1 complex mediates exosome formation in neuronal cells

Flo1 is also associated with exosome membranes [6]. To test whether exosome formation is affected by the depletion of LGI3/Flo1 complex, we prepared extracellular membrane fractions from siRNA-transfected cells. In contrast to control siRNA-transfected cells, the amount of Alix, another marker for exosome membranes, was significantly decreased in both cell lysates and extracellular membrane fractions from LGI3-depleted cells (Fig. 3). However, the depletion of LGI3 did not affect the amount of TfR (Fig. 3).

Discussion

In this study, we showed that LGI3 interacts with Flo1 in the brain and that the LGI3/Flo1 complex mediates APP trafficking and exosome formation. Co-immunoprecipitation analyses revealed that an approximately 70 kDa form of LGI3 interacts with Flo1 (Fig. 1b). A full-length LGI3 is considered to be an approximately 60 kDa protein [1,3], and an approximately 35 kDa truncated form of LGI3 is predominant in the Neuro2a cells (data not shown). Although additional investigations are needed, the truncated LGI3 might dimerize and then interact with Flo1 in the mouse brain. This idea would be supported by the recent finding that syntaxin-1 associates with an approximately 35 kDa truncated form of LGI3, not full-length LGI3, in the mouse brain [7].

Most notably, our RNA interference studies showed that the LGI3/Flo1 complex mediates APP trafficking in the neuronal cells (Fig. 2). As we showed earlier that LGI3 mediates Aβ and transferrin internalization [3], we first assumed that LGI3 is also involved in APP endocytosis. The depletion of LGI3 or Flo1 clearly decreased β-site cleavage products, indicating that APP endocytosis is disturbed (Fig. 2a and b). However, surprisingly, the depletion of LGI3 or Flo1 also decreased α-site cleavage products (Fig. 2b and c). α-site cleavage is considered to occur at plasma membranes before the endocytosis

Fig. 2

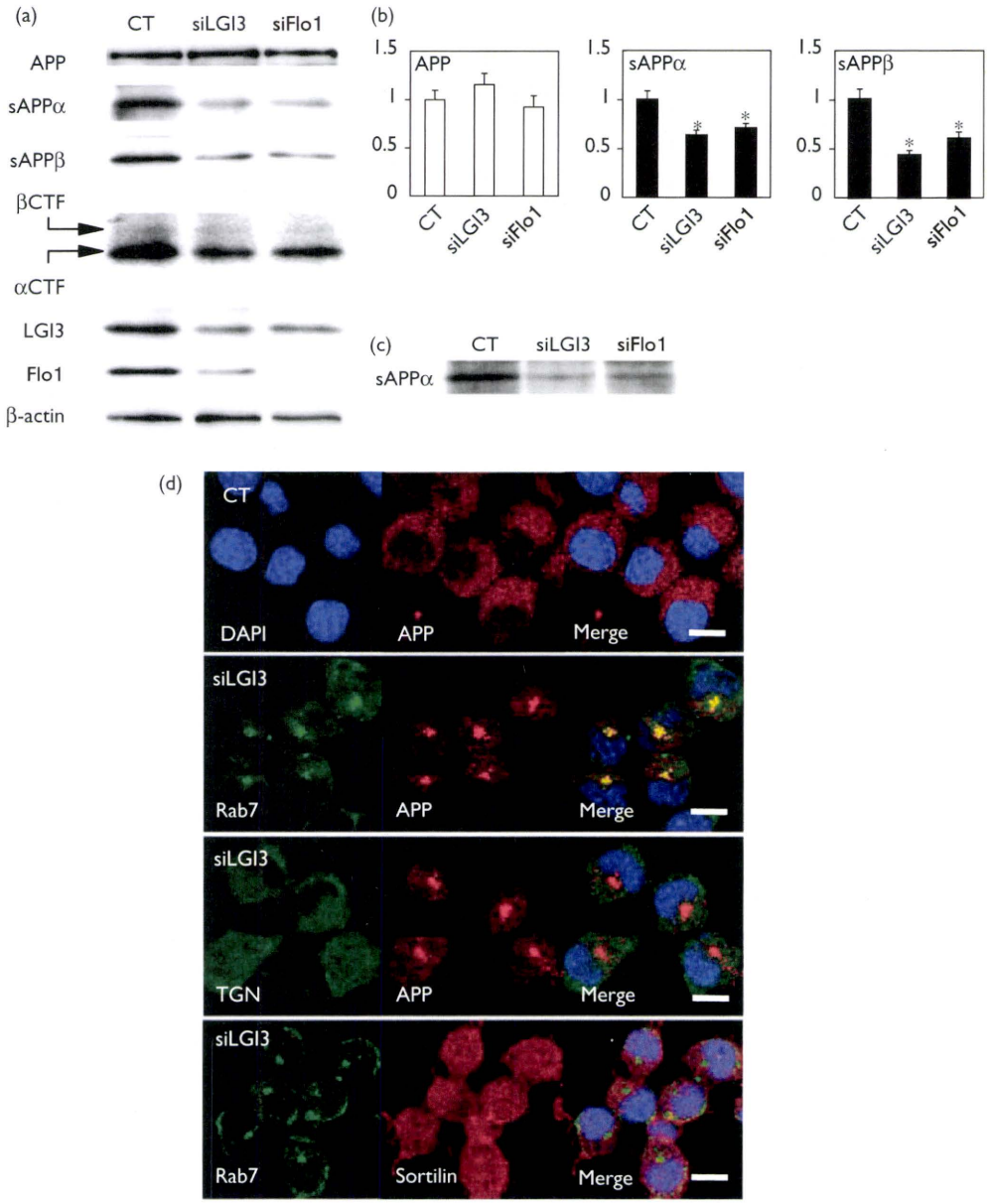

(a) Western blots showing the amount of APP, sAPPα, sAPPβ, αCTF, βCTF, LGI3, Flo1, and β-actin in Neuro2a cells 72 h after siRNA transfection. In LGI3- and Flo1-depleted cells, the amount of sAPPα, sAPPβ, αCTF, and βCTF was appreciably decreased. (b) Histograms showing the effect of LGI3 and Flo1 depletion on the amounts of full-length APP, sAPPα, and sAPPβ in Neuro2a cells. All data were normalized according to β-actin levels. Values are means ± SD. $*P<0.001$. Y-axes show the mean values of the quantified data. (c) Western blots showing the amount of sAPPα released into culture media 72 h after siRNA transfection. (d) Photomicrographs of Neuro2a cells 72 h after siRNA transfection. In siLGI3-transfected cells, APP clearly accumulated near the nucleus, localizing to Rab7-positive endosomes, however, sortilin remained unchanged. Scale bars, 10 μm.

of APP [11], suggesting that APP may not be trafficked to the plasma membrane as a result of the depletion of LGI3/Flo1 complex.

Immunocytochemistry showed that APP accumulated near the nuclei in LGI3-depleted cells, localizing to Rab7-positive endosomes, i.e., late endosomes (Fig. 2d). Cation-dependent mannose 6-phosphate receptor, a major late endosomal protein, is transported from the trans-Golgi network to late endosomes [12], suggesting that proteins can be transported directly to late endosomes from the secretory pathway. Western blot analyses confirmed that the molecular weight of full-length APP was approximately 110 kDa, even in LGI3-depleted or Flo1-depleted cells, suggesting that APP maturation through the secretory pathway is not disturbed. Thus,

Fig. 3

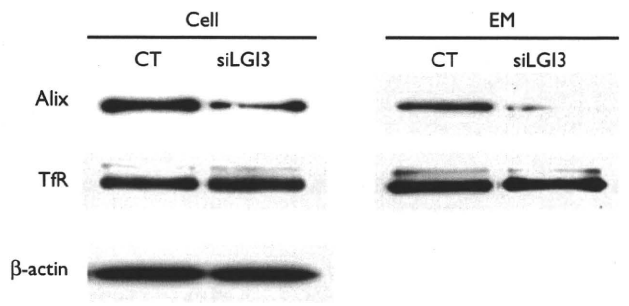

Western blots showing the amount of Alix, transferrin receptor (TfR), and β-actin in whole-cell extracts (Cell) and extracellular membrane (EM) fractions from Neuro2a cells 72 h after siRNA transfection. LGI3 depletion significantly decreased the levels of Alix in both Cell and EM. By contrast, LGI3 depletion did not affect the amount of TfR.

the depletion of the LGI3/Flo1 complex may alter APP trafficking from trans-Golgi network directly to late endosomes but not to the plasma membrane. Moreover, as the depletion of the LGI3/Flo1 complex did not alter the localization of another transmembrane protein, such as sortilin (Fig. 2d), the LGI3/Flo1 complex may mediate APP trafficking specifically.

As Flo1 is associated with exosome membranes [6], it is reasonable that LGI3 is also associated with exosome membranes. This would explain why LGI3 is detected as a secreted protein in the culture medium [13]. Moreover, the depletion of the LGI3/Flo1 complex significantly decreased the amount of Alix, another exosome membrane marker, in both cell lysates and extracellular membrane fractions (Fig. 3a). This finding suggests that the LGI3/Flo1 complex is required for exosome formation itself. As the depletion of LGI3 failed to affect the amount of TfR in the extracellular membrane fractions (Fig. 3), LGI3/Flo1 may not mediate the recycling endocytic pathway.

It is unclear how LGI3 is involved in CLA-dependent endocytosis. An earlier study showed that the depletion of Flo1 did not affect transferrin uptake in HeLa cells [5]. In this study, immunocytochemistry revealed that LGI3 partly colocalizes with CLA near the plasma membranes (Fig. 1a). Although additional investigations are needed, a population of LGI3 molecules may associate with CLA independently of Flo1, and these LGI3/CLA complexes might work only when endocytosis occurs. Overall, the results of this study suggest that LGI3 is involved not only in endocytosis but also in other intracellular transport systems through binding with co-factors such as Flo1.

Conclusion

LGI3 interacts with Flo1 in the brain, and LGI3/Flo1 mediates APP trafficking and exosome formation in neuronal cells. This line of research would provide a great contribution to reveal the details of the intracellular transport system and even the secretion pathway in the brain.

Acknowledgements

This study was supported by a grant-in-aid from the Ministry of Health, Labor, and Welfare, and the Ministry of Education, Culture, Sports, Science, and Technology, Japan.

References

1 Kimura N, Ishii Y, Suzaki S, Negishi T, Kyuwa S, Yoshikawa Y. Aβ upregulates and colocalizes with LGI3 in rat cultured astrocytes. *Cell Mol Neurobiol* 2007; **27**:335–350.
2 Glenner GG. Alzheimer's disease: its proteins and genes. *Cell* 1988; **2**:307–308.
3 Okabayashi S, Kimura N. LGI3 is involved in Aβ uptake by astrocytes and endocytosis itself. *Neuroreport* 2008; **19**:1175–1179.
4 Saavedra L, Mohamed A, Ma V, Kar S, De Chaves EP. Internalization of beta-amyloid peptide by primary neurons in the absence of apolipoprotein E. *J Biol Chem* 2007; **282**:35722–35732.
5 Glebov OO, Bright NA, Nichols BJ. Flotillin-1 defines a clathrin-independent endocytic pathway in mammalian cells. *Nat Cell Biol* 2006; **8**:46–54.
6 Rajendran L, Honsho M, Zahn TR, Keller P, Geiger KD, Verkade P, Simons K. Alzheimer's disease beta-amyloid peptides are released in association with exosomes. *Proc Natl Acad Sci U S A* 2006; **103**:11172–11177.
7 Park WJ, Lee SE, Kwon NS, Baek KJ, Kim DS, Yun HY. Leucine-rich glioma inactivated 3 associates with syntaxin 1. *Neurosci Lett* 2008; **444**:240–244.
8 Schneider A, Rajendran L, Honsho M, Gralle M, Donnert G, Wouters F, *et al.* Flotillin-dependent clustering of the amyloid precursor protein regulates its endocytosis and amyloidogenic processing in neurons. *J Neurosci* 2008; **28**:2874–2882.
9 Ehehalt R, Keller P, Haass C, Thiele C, Simons K. Amyloidogenic processing of the Alzheimer beta-amyloid precursor protein depends on lipid rafts. *J Cell Biol* 2003; **160**:113–123.
10 Fuentealba RA, Barría MI, Lee J, Cam J, Araya C, Escudero CA, *et al.* ApoER2 expression increases Abeta production while decreasing Amyloid Precursor Protein (APP) endocytosis: possible role in the partitioning of APP into lipid rafts and in the regulation of gamma-secretase activity. *Mol Neurodegener* 2007; **2**:14.
11 Sisodia SS. Beta-amyloid precursor protein cleavage by a membrane-bound protease. *Proc Natl Acad Sci U S A* 1992; **89**:6075–6079.
12 Rohrer J, Schweizer A, Johnson KF, Kornfeld S. A determinant in the cytoplasmic tail of the cation-dependent mannose 6-phosphate receptor prevents trafficking to lysosomes. *J Cell Biol* 1995; **130**:1297–1306.
13 Senechal KR, Thaller C, Noebels JL. ADPEAF mutations reduce levels of secreted LGI1, a putative tumor suppressor protein linked to epilepsy. *Hum Mol Genet* 2005; **14**:1613–1620.

BRAIN RESEARCH 1315 (2010) 137–149

available at www.sciencedirect.com

ScienceDirect

www.elsevier.com/locate/brainres

BRAIN RESEARCH

Research Report

Alzheimer-type tau pathology in advanced aged nonhuman primate brains harboring substantial amyloid deposition

Naoto Oikawa[a], *Nobuyuki Kimura*[b], *Katsuhiko Yanagisawa*[a,*]

[a]*Department of Alzheimer's Disease Research, National Institute for Longevity Sciences, National Center for Geriatrics and Gerontology, 36-3, Gengo, Morioka, Obu, Aichi 474-8522, Japan*

[b]*Laboratory of Disease Control, Tsukuba Primate Research Center, National Institute of Biomedical Innovation, 1-1, Hachimandai, Tsukuba-shi, Ibaraki 305-0843, Japan*

ARTICLE INFO

Article history:
Accepted 1 December 2009
Available online 8 January 2010

Keywords:
Alzheimer disease
Amyloid β-protein
Tau
Tau phosphorylation
Argyrophilic tangle
Dystrophic neurite
Cynomolgus monkey

ABSTRACT

We elucidated how Alzheimer-type pathologies of amyloid β-protein (Aβ) and tau spatiotemporally emerge in brains of nontransgenic nonhuman primate, cynomolgus monkey, in the present study. To examine the accumulation of deposited Aβ, phosphorylated tau accumulation, intracellular tau accumulation, and neurofibrillary tangle formation, the brains, mainly temporal cortex and hippocampus, of 34 cynomolgus monkeys aged 6 to 36 years were studied by biochemical and histochemical analyses. Biochemically, first, the accumulation of insoluble Aβ was detected in the neocortical (temporal and frontal) and hippocampal regions of animals as young as mid-20s and their levels were extremely high in those of advanced age. The accumulation of phosphorylated tau in the same regions occurred before the age of 20 with poor correlation to the levels of insoluble Aβ. Histologically, intraneuronal and intraoligodendroglial tau accumulation was observed in temporal cortex and hippocampus of animals before the age of 20. In an advanced aged 36-year-old individual, argyrophilic tangles and tau-accumulated dystrophic neurites were markedly observed in the medial temporal area contiguous to limbic structures. Notably, these tau pathologies also emerged, to a lesser extent, in the temporal cortices of advanced aged animals harboring significant amounts of insoluble Aβ. These results suggest that the cynomolgus monkey can be used to elucidate the age-dependent sequence of Aβ and tau pathologies.

1. Introduction

The emergence of numerous senile plaques (SPs), neurofibrillary tangles (NFTs), and neuronal loss are hallmarks of Alzheimer disease (AD). The main component of SPs is amyloid β-protein (Aβ), which is a 39- to 43-residue protein with heterogeneity at their carboxy-termini. Among them, Aβ40 and Aβ42 terminating at Val-40 and Ala-42, respectively, are major forms (Mori et al., 1992; Roher et al., 1993). On the other hand, NFTs are mainly composed of a microtubule-associated protein, tau (Grundke-Iqbal et al., 1986, Ihara et al., 1986), with hyperphosphorylation (Flament et al., 1989, Lee et al., 1991).

* *Corresponding author*. Fax: +81 562 44 6594.
E-mail address: katuhiko@ncgg.go.jp (K. Yanagisawa).

Abbreviations: AD, Alzheimer disease; Aβ, amyloid β-protein; SP, senile plaque; NFT, neurofibrillary tangle; APP, amyloid precursor protein; NHP, nonhuman primate

0006-8993/$ – see front matter © 2009 Elsevier B.V. All rights reserved.
doi:10.1016/j.brainres.2009.12.005

Fundamental questions regarding the pathogenesis of AD is how Aβ and tau are integrated into SPs and NFTs, respectively, and how these pathological assemblies are relevant to neuronal death. Moreover, it remains unclear whether the formations of SPs and NFTs are linked or mutually independent. To date, enormous efforts have been made to elucidate these issues using various animal models, particularly transgenic (Tg) mice. In the analysis of processes underlying Aβ pathology in AD, the Tg mice harboring the familial AD-related mutations in *amyloid precursor protein (APP)* gene and *presenilin* genes have been extensively studied (for review, Duyckaerts et al., 2008). In the analysis of processes underlying tau pathology in AD, alternative Tg mice harboring the mutations relating to other tauopathies, including frontotemporal dementia and parkinsonism linked to chromosome 17 (FTDP-17), in *tau* gene have been studied (for review, Frank et al., 2008). Furthermore, triple Tg mice harboring mutations in *APP*, *presenilin*, and *tau* genes are fascinating because these mice show synaptic dysfunction in addition to the formation of both SPs and NFTs (Oddo et al., 2003). These Tg mice are indeed valuable models for studying AD pathogenesis; however, it has been argued that the pathological sequences observed in these mice are different from those in AD brain. The differences may be attributed to alterations in the expression levels of APP and tau, which could occur through genetic manipulations. For example, Aβ is overproduced far beyond the physiological extent in APP-Tg mice owing to the enhanced expression of mutant APP, resulting in high loads of soluble Aβ prior to the development of any Aβ pathology (Kawarabayashi et al., 2001; Kuo et al., 2001).

Nontransgenic animals, such as nonhuman primates (NHPs) and nonprimate mammalian species, are also available for studying the pathogeneses of Aβ and tau. Distinct from Tg mice, both the production of Aβ and expression of tau are likely within physiological ranges in nontransgenic animals; thus, the natural spatiotemporal profiles of Aβ and tau pathologies should be presented in the brains of these animals. To date, it has been reported that a lot of mammalian species exhibit cerebral Aβ-amyloidosis, such as parenchymal Aβ deposition and amyloid angiopathy, and intraneuronal tau accumulation (Bons et al., 2006; Braak et al., 1994; Cummings et al., 1996a,b; Gearing et al., 1994; Geula et al., 2002; Härtig et al., 2000; Lemere et al., 2004, 2008; Podlisny et al., 1991; Roertgen et al., 1996; Schultz et al., 2000a,b; Selkoe et al., 1987; Walker et al., 1987). Among those animals, we paid particular attention to cynomolgus monkey because of the similarity of Aβ pathology as follows. First, cored plaque is the major type in the monkey brain (Nakamura et al., 1998). Second, the number of Aβ42-composed plaques is higher than that of Aβ40-composed ones in the parenchyma, whereas the amyloid angiopathies are equally immunostained with anti-Aβ42 antibody and anti-Aβ40 antibody, respectively (Nakamura et al., 1995). However, it has not been clarified whether Aβ is deposited in the brain in age-dependent and region-specific manners. Tau pathology has also been previously studied in cynomolgus monkey brain (Kiatipattanasakul et al., 2000; Kimura et al., 2003, 2007; Nakamura et al., 1996a,b). Among them, tangle formation in neurons and glial cells was reported in one case although this case may be atypical because the animal showed some neurological deficit and tangles were detected only in subcortical regions (Kiatipattanasakul et al., 2000). Despite these previous studies, it remains to be determined whether Aβ pathology and tau pathology in the brain independently occur or are mutually related in cynomolgus monkey brains.

In this study, we biochemically and histologically characterized the profiles of Aβ and tau pathologies in detail in the brains of cynomolgus monkeys aged 6 to 36 years old. Here, we report that Alzheimer-type tau pathology can occur in advanced aged brains, even in neocortices, harboring substantial amounts of insoluble Aβ.

2. Results

2.1. *Age-dependent and region-specific insoluble Aβ deposition in the brains*

To determine whether Aβ deposition occurs in age-dependent and region-specific manners in the brains of NHP, we biochemically examined 33 temporal cortices and 19 hippocampi obtained from monkeys aged from 6 to 36 years (temporal cortices) and from 17 to 36 years (hippocampi). In a serial Western blotting analysis of those, insoluble Aβ was initially detected in the animals in their mid-20s, whereas insoluble Aβ was not detectable in animals under the age of 22 years in temporal cortices and of 24 years in hippocampi (Fig. 1A. The data for animals aged 6 and 14 years are not shown). In general, accumulation of insoluble Aβ occurred in an age-dependent manner; however, the levels of insoluble Aβ were variable from animal to animal. Some animals even over the mid-20s did not show any Aβ deposition. Notably, the level of insoluble Aβ was extremely high in two animals over the age of 30 (32-c and 36-c). To confirm the result of biochemical examination, we performed immunohistochemistry on the temporal cortices of the animals under the age of 20 (17-a), mid-20s (25-b), and over the age of 30 (32-c and 36-c). In accordance with the results of biochemical analysis, the immunohistochemical study revealed a small and large number of Aβ-immunoreactive plaques in the sections of the animal aged 25 years (25-b) and over the age of 30 (36-c), respectively, whereas no Aβ-immunoreactivity was observed in the animal aged 17 years (17-a) (Fig. 1B). In addition to the samples of the temporal cortex and hippocampus, we also biochemically examined the insoluble Aβ in the frontal and occipital cortices and cerebellum of the animals in their mid-20s. The levels of insoluble Aβ were high in the samples of frontal and temporal cortices, whereas that of the occipital cortices was very low (Fig. 1C). On the other hand, no insoluble Aβ were detected in the cerebella (Fig. 1C).

2.2. *Level of soluble Aβ in the brains*

Soluble fraction of brain homogenates were analyzed to detect soluble Aβ on 16 temporal cortices and 9 hippocampi of the animals aged from 14 to 36 years (temporal cortices) and from 25 to 36 years (hippocampi). Soluble Aβ was not detected in the most analyzed samples; however, the Aβ was detected only in the animals over the age of 30, which showed extremely high levels of insoluble Aβ deposition (Supplemental Fig. 1A). The

data for animals aged from 14 to 24 years are not shown. To explore the source of the soluble Aβ and estimate the contribution of the levels of soluble Aβ to the deposition of insoluble Aβ in the brain, we performed Western blotting analyses of soluble and insoluble fractions obtained from identical samples of brains of monkeys aged over 30 and of APP-Tg mice, Tg2576, aged 13.5 months. In contrast to the sample of APP-Tg mouse brains, in which comparable levels of soluble and insoluble Aβ were detected, soluble Aβ was detected at only negligible levels, despite the extremely high levels of insoluble Aβ, in the samples of monkey brains (Supplemental Fig. 1B).

2.3. *Deposited, insoluble Aβ species in the brains*

To determine which species of Aβ initially and favorably deposited in the monkey brains, we performed Western blotting analysis using the anti-Aβ40 and Aβ42 antibodies in the temporal cortices of five animals aged 24 to 32 years. In accordance with the result of a previous report (Nakamura et al., 1995), the levels of insoluble Aβ42 were apparently higher than those of Aβ40 in almost all samples except one, 25-c, in which the levels of Aβ42 and Aβ40 were comparable (Supplemental Fig. 2A). In the Western blotting using an anti-pyroglutamate Aβ (N3pE-Aβ) antibody (Supplemental Fig. 2B), the immunoreactivity was detected at a significant level only in the sample obtained from the animal aged 32 years, 32-c, which contained an extremely high level of insoluble Aβ42 (Supplemental Fig. 2A).

2.4. *Accumulation of soluble phosphorylated tau in the brains*

We performed Western blotting analysis of the soluble fractions of the temporal cortex and hippocampus using 2B11, and then we assessed the levels of tau phosphorylation by estimating the mobility shift of the immunoreactive bands based on the results of the samples that were treated for enzymatic dephosphorylation prior to Western blotting (Fig. 2A). With this procedure, it was revealed that phosphory-

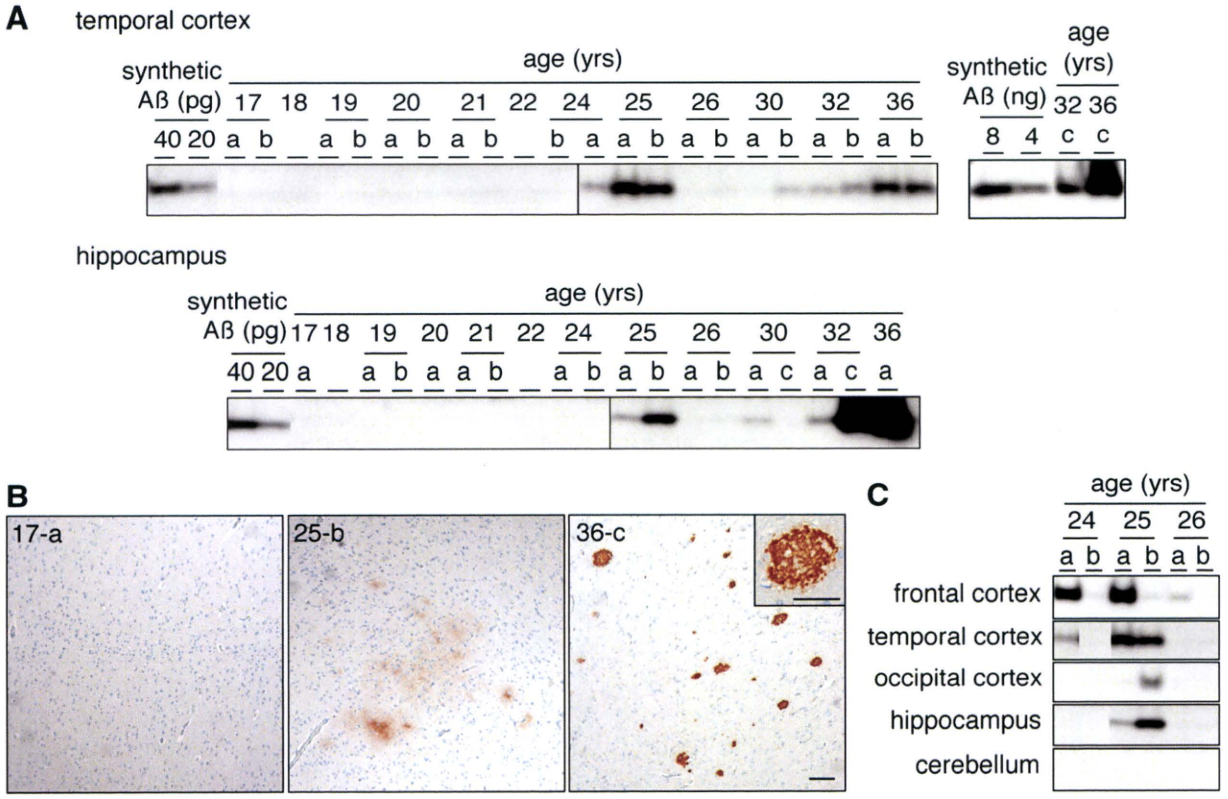

Fig. 1 – Age-dependent and region-dependent insoluble Ab deposition in monkey brains. (A) Western blots of TBS-insoluble Aβ in the samples of temporal cortices (upper panels) and hippocampi (lower panel) of cynomolgus monkey brains. Samples from monkeys aged 17 to 36 years were analyzed. Note that only two samples of temporal cortices, 32-c and 36-c, were examined in a normal manner, not in a highly sensitive manner, so that the order was different from the other blots (upper right panel). The small letters (a, b, and c) written under the ages indicate individual monkeys. (B) Immunohistochemistry using anti-Aβ antibody [anti-human amyloid β (N)] in temporal cortices of 17-a, 25-b, and 36-c. Scale bar, 50 μm (inset of 36-c) and 100 μm. (C) Western blots of TBS-insoluble Aβ in the samples of frontal, temporal, and occipital cortices, hippocampus, and cerebellum. The samples from monkeys aged 24 to 26 years were analyzed. The panels of temporal cortex and hippocampus are the same as those of panel A. In Western blotting, the applied samples were normalized to the tissue wet weight (0.3 mg/sample). Aβ band at 4 kDa was detected using 6E10. Synthetic Aβ1-40 was loaded in each blot.

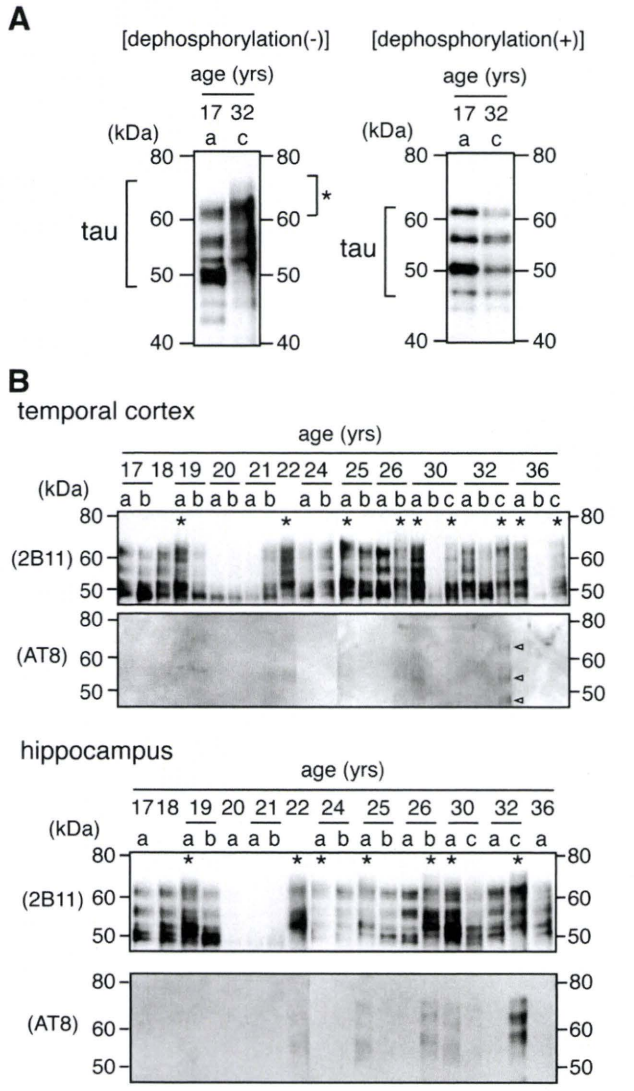

Fig. 2 – Phosphorylation state of TBS-soluble tau in the temporal cortex and hippocampus of monkey brains. (A) Representative pictures of Western blots of hippocampal samples using anti-tau antibody (2B11). Tau bands are indicated by a black square bracket on the left side. The mobility shifts of bands were assessed focusing on the area indicated by an asterisk (left panel). On the same samples, dephosphorylated samples were blotted (right panel). The small letters (a, b, and c) written under the ages indicate individual monkeys. (B) Western blots using 2B11 (upper panel), and anti-phospho-tau antibody, AT8 (lower panel), of the temporal cortical and hippocampal samples without dephosphorylation prior to Western blotting. Asterisks indicate the individuals in whom the mobility shifts of tau bands, mentioned in panel A, were observed. Arrowheads in the blot of the temporal cortical samples indicate AT8-immunoreactive bands.

lated tau accumulated in both the temporal cortex and hippocampus of the brains of animals before the age of 20 (Fig. 2B). We also performed Western blotting using AT8 to search for tau phosphorylation. The AT8-reactive bands were detected in several samples, in which accumulation of phosphorylated tau was also observed using 2B11, and the intensity of AT8-reactive bands increased in an age-dependent manner in the hippocampus (Fig. 2B).

To correlate between the levels of deposited Aβ and accelerated tau phosphorylation (Table 1), the accumulation of phosphorylated tau preceded Aβ deposition as a function of age both in the temporal cortex and hippocampus. Moreover, the accumulation of phosphorylated tau appeared to be independent of the level of Aβ deposition in the monkey brain. However, it was intriguing that abnormally phosphorylated tau, which was detected using AT8, only significantly accumulated in the brains showing extremely high levels of Aβ deposition.

2.5. *Intracellular accumulation of tau in the brains*

To examine the accumulation of tau in the cell with age, we performed immunohistochemical analysis of total tau using 2B11. In the case of 17-a, in which the accumulation of phosphorylated tau, which was determined by the mobility shift of 2B11-reacted tau bands, was negligible in the Western blotting (Fig. 2B), no 2B11 immunoreactivity was observed in the temporal cortex (Fig. 3A) or the hippocampus (data not shown). Whereas in 19-a, in which the accumulation of phosphorylated tau was observed in the Western blotting, the 2B11 immunoreactivity was readily observed in a considerable number of neurons and some glial cells, in the temporal cortex (Fig. 3B) and the hippocampus (data not shown). In animals over the age of 20 (26-a, 26-b, 32-a, 32-c, and 36-c), the number of 2B11-positive glial cells increased with age in good accordance with the result of Western blotting (Figs. 2B and 3C, Table 2). However, 2B11-positive neurons were not detected in the sections of the animals aged over 20 except 36-c, in which strong 2B11 immunoreactivities were occasionally observed in neurons, glial cells, and in clustered dystrophic neurites in the temporal cortex (Figs. 3E–G). The same immunostaining pattern was obtained with HT7, which recognizes residues positioned from 159 to 163 of tau and is expected to detect total tau (data not shown). To characterize 2B11-positive glial cells, we performed double immunostaining of total tau and GFAP (glial fibrillary acidic protein) or Olig2 as markers for astrocytes and oligodendrocytes, respectively. Nearly all 2B11-immunopositive glial cells were Oilg2 immunoreactive (Fig. 3D) and devoid of GFAP immunoreactivity (data not shown).

To investigate whether phosphorylated tau is accumulated in the cell, we also performed immunohistochemical analysis using AT8, which selectively recognizes abnormally phosphorylated tau, in the temporal cortices and hippocampi of the animals, examined in the experiment shown in Fig. 4. In the samples from animals under the age of 30, AT8 immunoreactivity was not detected except in 26-b, in which faint immunoreactivities were detected in a moderate number of glial cells in the temporal cortex, particularly in deeper layers (Fig. 4A). The number of glial cells with the faint immunoreactivities with AT8 in the temporal cortex of 32-c was larger than that of 26-b (26-b, about 34 cells/mm^2; 32-c, about 90 cells/mm^2). Those AT8-positive glial cells were also immunostained with anti-Olig2 antibody but not with anti-GFAP antibody

Table 1 – Biochemical and quantitative profile of Aβ deposition and tau phosphorylation in the brain homogenates.

		19-a	22	24-a	25-a	25-b	26-b	30-a	32-a	32-b	32-c	36-a	36-c
Temporal cortex	Aβ	–	–	+	++	++	–	–	+	+	+++	++	+++
	tau	+	+	–	+	–	+	+	–	–	+*	+	+
Hippocampus	Aβ	–	–	–	+	++	–	+	+	NE	+++	+++	NE
	tau	+	+*	+	+**	–	+**	+**	–	NE	+***	–	NE

The amount of deposited Aβ, that is investigated in Western blotting analysis using 6E10, in the samples is indicated as follows: –, negligible; +, slight; ++, moderate; +++, remarkable. Presence or absence of tau phosphorylation, which was determined with the mobility shift of the 2B11-immunoreactive bands, is indicated as (+) or (–), respectively. Asterisks indicate the levels of AT8 immunoreactivities: *, slight; **, moderate; ***, remarkable; NE, not examined.

(data not shown). In the temporal cortex and hippocampus of 32-a, a neurite-like structure and glial cells were occasionally immunostained with AT8 (Fig. 4B). Notably, the immunostaining of glial cells was strong. In addition, clustered dystrophic neurites were also detected with AT8 in the temporal cortex of 32-c (Fig. 4C). Moreover, some neurons were strongly immunostained with AT8 in the temporal cortex of 36-c (Fig. 4D).

2.6. *Formation of argyrophilic structures in the advanced aged monkey brains*

To explore the formation of argyrophilic tangles in monkey brains, we performed Gallyas silver staining, which is known to be a highly specific silver-staining method for detecting NFTs (for a review, see Uchihara, 2007) of the temporal cortices

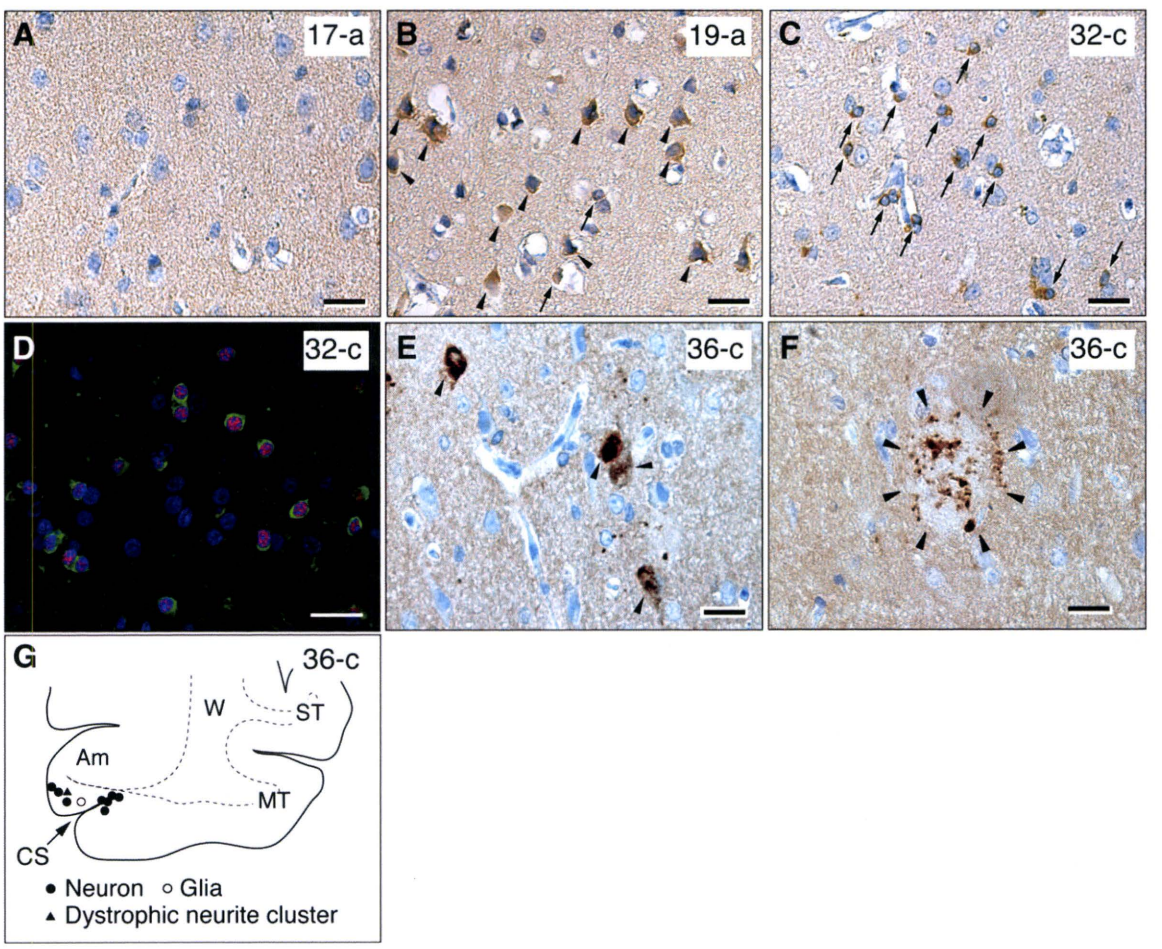

Fig. 3 – Accumulation of tau in neurons and glial cells in the temporal cortices of monkey brains. (A-C, E, and F) Immunoperoxidase staining of temporal cortices using 2B11 with counterstaining using hematoxylin. A, 17-a; B, 19-a; C, 32-c; E and F, 36-c. Arrows and arrowheads indicate 2B11-positive glial cells and neurons, respectively. 2B11-positive dystrophic neurite cluster is indicated by arrowheads. (D) Double immunofluorescence labelling of temporal cortex of 32-c using 2B11 (green) and anti-Olig2 antibody (red), which reacts with nuclear protein, Oilg2, of oligodendrocytes. Nuclei were stained with DAPI (blue). Scale bar, 20 μm. (G) Distributions of 2B11-positive neuron (•), glial cell (○), and dystrophic neurite cluster (▲) in the brain of 36-c. W, white matter; ST, superior temporal gyrus; MT, middle temporal gyrus; Am, amygdala; CS, collateral sulcus.

Table 2 – Glial immunoreactivities with 2B11 in the brains.

	17-a	19-a	26-a	26-b	32-a	32-c	36-c
Temporal cortex	–/+	+	+	++	+	+++	+
Hippocampus	–/+	–/+	+	NE	+	++	NE

The analysis for counting the number of 2B11-positive glial cells was performed as described in Experimental procedures. The number of 2B11-immunoreactive glial cells per mm^2 is indicated as follows: –/+, 1 to 30; +, 31 to 100; ++, 101 to 300; +++, 300 <; NE, not examined.

and hippocampi of animals over the age of 20. Whereas Gallyas silver staining was absent in the samples of 26-a, 26-b, and 32-a, argyrophilic tangles were detected in a neuron of the temporal cortex of 32-c (Fig. 4E). In the temporal cortex of 36-c, a moderate number of argyrophilic tangles was found in neurons, glial cells, and clustered dystrophic neurites by Gallyas silver staining (Figs. 4F, G). Almost all of them were located at the medial temporal areas adjacent to the amygdala (Fig. 4H). Distribution patterns of AT8 immunoreactivity and Gallyas silver staining in the brains of 32-a, 32-c, and 36-c are shown in Fig. 4H.

To examine the formation of paired helical filament (PHF), which is a unit fibril of NFT, in the monkey brains, we biochemically investigated the insoluble tau on the hippocampus of the animals aged 6, 17, 19, 25, and 32 years. However, we could not detect PHF even in the brain of the animal aged 32 years, 32-c (data not shown).

3. Discussion

Here, we showed that Aβ deposition occurred in cynomolgus monkey brains in age-dependent and region-specific manners, essentially resembling the deposition behavior of Aβ in human brains, both in normally aged individuals and patients with AD. The accumulation of phosphorylated tau was also observed; however, it started with poor correlation to the levels of Aβ deposition in the brain. Notably, Alzheimer-type tau pathology, including the formation of argyrophilic tangles and tau-accumulated dystrophic neurites, emerged predominantly in the medial temporal regions, and to a lesser extent, in the temporal cortices of the brains of advanced aged animals, which showed extremely high levels of Aβ deposition. The present findings make it attractive to use aged cynomolgus monkey brains to elucidate the mechanism and pathological significance of Aβ and tau pathologies.

In AD brains, it has been reported that the frontal and temporal cortices are the initial and favorable regions for Aβ deposition, whereas the occipital cortex and cerebellum are unfavorable regions for Aβ deposition (Braak and Braak, 1991; Näslund et al., 2000). The present study showed that the region specificity of age-dependent Aβ deposition in the monkey brains is similar to that of AD brain. In addition, extremely high levels of deposited Aβ were accompanied with rather low levels of soluble Aβ in the monkey brains as is the case in AD brains. It must be noted that the levels of soluble Aβ in the Tg mouse brains are extremely high compared with those in AD and monkey brains. Thus, although we do not intend to underestimate the usefulness of Tg mice to study Aβ pathogenesis, the use of nontransgenic animals, including cynomolgus monkey, is advantageous for studying the *bona fide* sequence of Aβ pathology, which can take place under particular conditions such as aging without the prior enhancement of Aβ production. In regard to the Aβ species that favorably deposits in the brains, attention has been paid to N3pE-Aβ (Hosoda et al., 1998; Iwatsubo et al., 1996; Saido et al., 1995, 1996). In the animals including transgenic mice, N3pE-Aβ was detected although its level was not necessarily high in the brains (Kawarabayashi et al., 2001; Kuo et al., 2001; Tekirian et al., 1998). In this study, a significant level of deposited N3pE-Aβ was only detected in the advanced aged monkey brain. Thus, although previous studies suggest that N3pE-Aβ may be a species that is prone to initially deposit in AD brain (Hosoda et al., 1998; Iwatsubo et al., 1996; Saido et al., 1995, 1996), our result suggests that, at least in monkey brains, N3pE-Aβ is generated by the conversion of the full-length Aβ following its deposition.

One of the interesting findings of this study is that the numbers of 2B11-positive neurons in the brains of animals over age of 30 were smaller than those in the brain of a 19-year-old animal. In contrast to this, the numbers of 2B11-positive oligodendroglial cells increased with age. Although we cannot exclude the possibility that the 19-year-old animal was an unusual case, it may be possible to speculate that the reduction of the 2B11 immunoreactivity in neurons reflects the failure of recognition by 2B11 owing to the conformational change of tau at its epitope region. In support of this possibility, it is noteworthy that tau likely adopts a specific conformation under the pathological condition (Jeganathan et al., 2008) or/and begins to assemble based on the particular sequence motif, ^{306}VQIVYK^{311}, which is included in the 2B11 epitope region (Von Bergen et al., 2000). If this is the case, we can explain why neurofibrillary tangle formation preferably occurs in neurons but not in glial cells in AD brains. In this

Fig. 4 – Accumulation of phosphorylated tau and formation of argyrophilic structure in the temporal cortices of advanced aged monkey brains. (A–D) Immunohistochemistry of the temporal cortices using AT8 with counterstaining using hematoxylin. (A) Faint AT8-positive glial cells (allows) of 26-b. (B) Strong AT8-positive glial cells and dystrophic neurites (inset) of 32-a. (C) Faint AT8-positive glial cells (arrows) and AT8-positive dystrophic neurite cluster (indicated by arrowheads) of 32-c. (D) Strong AT8-positive neurons of 36-c. (E–G) Gallyas silver staining. (E) A neuron with Gallyas-silver-positive structures of 32-c. (F) A neuron with Gallyas-silver-positive structures of 36-c. (G) A glial cell (arrow) and dystrophic neurite cluster (indicated by arrowheads) of 36-c. Scale bar, 20 μm. (H) Distributions of AT8-positive neuron (•), glial cell (○), dystrophic neurite (r), dystrophic neurite cluster (▲), Gallyas-silver-positive neuron (■), glial cell (·), and dystrophic neurite cluster (★) in the brains of 32-a, 32-c, and 36-c. W, white matter; ST, superior temporal gyrus; MT, middle temporal gyrus; Am, amygdala; Hi, hippocampus; CS, collateral sulcus.

context, a challenging and intriguing subject in future studies is to elucidate how the 2B11 epitope is involved in tau assembly and why the conformational change at the region of the 2B11 epitope selectively occurs in the intraneuronal milieu. A previous study showed that casein kinase 1, which is one of the expected tau protein kinases, is associated with NFTs but not with tau-containing glial inclusions in the brain with tauopathy including AD (Schwab et al., 2000). Given this